

Dependence of Warm and Cold Climate Depiction on Climate Model Resolution

DAVID RIND

Goddard Space Flight Center, Institute for Space Studies, New York, New York

(Manuscript received 25 February 1988, in final form 22 June 1988)

ABSTRACT

Climate model results are now being used to assess the potential societal impact of climate change, and to compare with paleoclimate indicators. The models used for these purposes currently employ relatively coarse resolution, and a key question is how the results might change as resolution is improved. To examine this issue, doubled-CO₂ and ice age simulations with boundary conditions identical for two different resolutions are run with the GISS model. The resolution dependency of climate change sensitivity, atmospheric dynamics, and regional climate depiction are discussed.

The results show that model resolution affects two key processes in the control runs, moist convection and the nonlinear transfer of kinetic energy into the zonal mean flow. The finer resolution model has more penetrative convection but less convection overall, aspects which alter its temperature and wind structure relative to those of the coarser grid model. With finer resolution there are also stronger winds, more evaporation and a more active hydrological cycle. While some of these changes are not particularly large, their characteristics are mirrored in the warm and cold climate simulations.

In comparison with the coarser resolution model, the finer grid doubled CO₂ run has a greater decrease in high-level cloud cover, eddy energy, and eddy energy transports, and a greater increase in atmospheric temperature, surface winds, precipitation, and penetrative convection. The ice age finer grid run shows the opposite effects when compared with the medium grid: greater eddy energy and eddy transport increases, greater reduction in hydrologic cycle and atmospheric temperature. Regional climate changes also differ with resolution, due to both the local expression of the different dynamical responses and the differing spatial possibilities. The development of higher resolution models, and the practical use of climate change results, should incorporate an awareness of the potential impact of resolution on model processes and climate change depiction.

1. Introduction

General circulation models have made the transition from a use in exploration of atmospheric dynamics to their current role of evaluating the climatic influences of potential perturbations (e.g., CO₂ changes). With the possible proximity of severe greenhouse-induced climate alterations, these models are now being asked to perform a more exacting function: generate realistic scenarios for regional changes. The model results are then to be used in assessment programs, such as that organized by the United States Environmental Protection Agency, with the potential economic impact of the changes reported to Congress. Model output is also used for paleoclimate studies to organize and substantiate climatic interpretations of geophysical indicators, such as pollen and lake levels.

The climate models which are providing climate change analysis in the EPA program, and have been used in the paleoclimate studies, have resolutions on the order of 4.5° by 7.5° [the equivalent grid box resolution in latitude by longitude of models used at the

National Center for Atmospheric Research (NCAR) and the Geophysical Fluid Dynamics Laboratory (GFDL)], or 8° × 10° [for the Goddard Institute for Space Studies (GISS)]. A question of obvious importance in this regard is the possible impact of model resolution on the results being presented.

Various studies have been made of the effect of model resolution on its simulation characteristics. Manabe et al. (1970) noted that the higher resolution (GFDL) models produce greater energy in the longest planetary waves (wave numbers less than 5), a result duplicated with the NCAR GCM (Wellck et al. 1971). Miyakoda et al. (1971) documented the improvement in a GFDL model weather forecast when run for more than 6 days with fine (approximately 1.25°) resolution. Current weather forecasting models use horizontal resolutions on the order of 0.8° in the nested grid domain (e.g., Hoke 1987).

In light of these developments, it may be surprising to those not closely involved in the field to discover that the climate models still utilize such coarse resolution. One explanation is that the computer time necessary to integrate high resolution climate models for the extended duration required to reach equilibrium (on the order of 30 model years for oceanic mixed layer depths of 65 m) becomes prohibitive as resolution is

Corresponding author address: Dr. David Rind, Goddard Space Flight Center/NASA, Institute for Space Studies, 2880 Broadway, New York, New York 10025.

increased. However, even runs of several years duration with specified sea surface temperatures do not employ very high resolution, among the finest being the recent use of the British Meteorological Office (UKMO) model at 300 km spatial scale (Mitchell et al. 1987). As noted by Welck et al. (1971), and Baer and Alyea (1971) with a quasi-geostrophic forced general circulation model, an improvement in model resolution results in an increase in zonal kinetic energy at the expense of the eddy kinetic energy, an intensification and poleward movement of the jet stream, and an increase of long wave energy at the expense of shorter waves. These changes produce more realistic models when resolution is first increased, but further reductions in scale continue the tendencies noted above, until unrealistic simulations result (e.g., Manabe et al. 1979; Palmer et al. 1986). Efforts are currently underway to introduce additional dissipation mechanisms, such as gravity wave drag (e.g., Palmer et al. 1986; McFarlane 1987; Rind et al. 1988) to improve higher resolution or upper atmosphere model simulations.

The consequence of the problems in formulating higher resolution models, and the computer time involved in their execution, has been to limit the climate change studies to resolutions of relatively coarse order. There have been a few attempts to quantify the difference in climate change due to a difference in model resolution. Palmer and Mansfield (1986) compared the impact of El Niño perturbations in the UKMO $2.5^\circ \times 3.75^\circ$ model with a coarser NCAR GCM; they found that results were dependent upon model climatology, particularly the weaker zonal flow in the coarser grid model. Kutzbach and Guetter (1987) noted that the 9k B.P. (before present) simulations with the NCAR CCM were similar to those of a different, lower resolution model (Kutzbach and Otto-Bliesner 1982). The result implied that if the forcing were strong enough (in this case the summertime solar radiation maximum at 9k B.P.), the models would act in a similar fashion. Mitchell et al. (1987) investigated the response of two different UKMO models to a 2°C warming of the sea surface temperature and doubled CO_2 . While the horizontal resolution was relatively similar in the two models, the vertical resolution and model physics differed. The precipitation changes resulting from the perturbation experiments differed between models in a manner similar to the differences between the control runs (a result which will be strongly echoed and expanded upon here). There has been no previous reported study looking in detail at the changes produced in the same model when run with different horizontal resolution.

Resolution dependency could result from several influences. Models with different resolutions are to some extent different models, with possible different inherent model sensitivities to climate change. Or, even with similar sensitivities, the models might produce different regional depictions. Results of climate per-

turbations are determined by comparison with the control run, so differences in either the control run or the experiment would be sufficient to produce different regional changes. Furthermore, basic dynamical properties such as jet stream location and Hadley Cell extent result from different balances among the thermal and momentum forcing terms (e.g., Rind and Rossow 1984; Rind 1986), and the balances might change with resolution.

To explore these issues, climate change simulations run with two different resolutions of the GISS model are used to investigate radiative, dynamical, and regional sensitivities to model grid size. Both cold and warm climates will be investigated because modeling results are applied to both past and future situations, and also to allow the effects a broader range of expression. In this study, we focus on the influence of resolution when the climate change magnitude is forced to be the same, by the use of identical changes in sea surface temperatures (and in the ice age experiments, land ice). This procedure isolates the effects of resolution independent of the additional changes which would accompany different magnitudes of global warming or cooling. Nevertheless, we will be able to comment on the likely influence of model resolution on model climate sensitivity.

2. Models and climate experiments

The two GISS model resolutions employed are 8° by 10° and 4° by 5° . These resolutions span the scales of the commonly used GFDL and NCAR models. A description of their climatology has been given in Hansen et al. (1983) and Rind (1986, 1987a,b); we refer to the $8^\circ \times 10^\circ$ as "medium," to be consistent with the previous publications, and the $4^\circ \times 5^\circ$ is referred to as "finer." A more detailed documentation of model results on the different scales is documented elsewhere (Druyan and Rind 1988). Both produce reasonable temperature simulations throughout the troposphere. The finer-resolution model generates a better depiction of the synoptic features, eddy momentum transport, and the Ferrel cell, due, presumably, to its better approximation of the governing differential equations and dynamic convergences. The coarser-resolution model has more realistic rainfall rates in tropical regions, due, most likely, to the fact that the moist convection scheme was developed for this resolution. Additional differences between the models are discussed in the presentation of results.

The warm climate simulations used will be those for doubled CO_2 . The results for the medium-resolution model were presented in Hansen et al. (1984), and Rind (1986). The sea surface temperatures generated by this model were interpolated to the finer resolution and run at $4^\circ \times 5^\circ$ with doubled atmospheric CO_2 (Rind 1987b). As similar sea surface temperatures were used in both resolutions, the annual global average surface

air temperature changes from the control runs were similar, approximately 4.2°C . The medium-resolution results are averages over 10 years, while the finer grid results are averages over 3 years.

The cold climate simulations are those of the Last Glacial Maximum, approximately 18,000 B.P., using the land ice and ocean temperature boundary conditions generated by CLIMAP (1981), along with the appropriate orbital parameters. Results for the medium grid run have been presented in several different publications (Hansen et al. 1984; Rind and Peteet 1985; Rind 1986, 1987a), while results for the finer-grid model have not previously been published. The medium-grid values are averages over 5 years, while the finer grid results are averages over 3 years.

Standard deviations for the annual mean or appropriate season are presented in several of the tables to indicate the degree of natural model variability independent of climate change. The standard deviations for the medium grid were generated from a 100-yr control run for the present climate which allowed the sea surface temperatures to change. The values thus slightly overestimate the model variability for the runs with specified sea surface temperatures. The variability for the finer grid comes from the 5-yr control run for the ice age experiments (with specified sea surface temperatures). For efficiency in presentation, the medium-grid standard deviations are shown in the tables with the warm climate results, and the finer-grid values with the cold climate results. The 4°C global warming and cooling in the experiments produce a variety of changes which are statistically significant (see also Rind 1986, 1987a), and the same is true of differences between resolutions. In all cases we attempt to trace the results to specific model processes, to help understand the physical changes which are occurring.

One additional feature of the comparison is that the warm and cold climate experiments have slightly different control runs. The medium-grid doubled CO_2 run used a present climate simulation that allowed the sea surface temperatures to change, but kept them close to observed values by incorporating specified ocean transports (Hansen et al. 1984). The finer-grid control run for doubled CO_2 also used these sea surface temperatures (interpolated to the finer resolution). Although the values are close to the specified (observed) temperatures used in the cold climate control runs, they are not identical. For this reason, results from the respective control runs will be shown in the individual tables, from which it will be apparent that the differences are generally small. The two sets of control runs provide a test of the consistency of resolution dependent effects in the current climate simulations.

All the specified sea surface temperature runs (the finer grid doubled CO_2 experiment and control, as well as the ice age experiments and controls) have at least a 1 year spinup prior to averaging of the results, while the medium grid doubled CO_2 experiment and its con-

trol were run for 25 years, before averaging over the last 10 years to define the equilibrium. The different model runs and averaging periods are given in Table 1.

3. Results

a. Climate sensitivity

1) GLOBAL RESPONSE

The dependence of the global climate sensitivity on model resolution cannot be evaluated precisely for any of the runs with specified sea surface temperatures (which restrict the model response), but an estimate can be obtained from the radiation balances. Relevant quantities are given in Table 2. The difference between the medium grid doubled CO_2 experiment and control run "net radiation at the top" of the atmosphere, indicated in Table 2a, is $7.9 - 7.5 = 0.4 \text{ W m}^{-2}$. As these runs were in approximate equilibrium, i.e., the sea surface temperature adjustment was complete, the excess radiation coming into the atmosphere in the doubled CO_2 run did not lead to a further rise in temperature but was being lost by processes such as melting of land ice, and runoff of heat with precipitation. The difference in the net radiation at the top for the finer grid doubled CO_2 experiment minus control is $10.2 - 9.7 = 0.5 \text{ W m}^{-2}$, close to the medium-grid result. Examination of the loss processes indicates they are similar to those for the medium grid. Thus, the doubled CO_2 climate sensitivity of the finer-grid model, on the global average, appears similar to that of the medium grid.

The situation for the ice age experiments is somewhat different. The net radiation at the top of the atmosphere in the medium grid ice age run is $-1.6^{\circ} \text{ W m}^{-2}$ less than its control run (Table 2b). The effect of this deficit can be approximated by considering that instantaneous doubling of CO_2 produces, after a few months, a net imbalance of about 4 W m^{-2} ; for the GISS medium grid model sensitivity, the result of this excess is the eventual 4.2°C equilibrium warming. With this example as a measure of the ratio of global temperature change to net radiative forcing, the ice age imbalance implies that were the sea surface temperatures allowed to change, the ice age run would have cooled by 1° to 2°C (Hansen et al. 1984). The finer-grid runs have a net imbalance of only 0.3 W m^{-2} , which would imply

TABLE 1. Climate model control runs and experiments.

Climate	Resolution	Years averaged	Sea surface temp
Present	$4^{\circ} \times 5^{\circ}$	3	Specified
Present	$8^{\circ} \times 10^{\circ}$	10	Calculated
2 CO_2	$4^{\circ} \times 5^{\circ}$	3	Specified
2 CO_2	$8^{\circ} \times 10^{\circ}$	10	Calculated
Present	$4^{\circ} \times 5^{\circ}$	5	Specified
Present	$8^{\circ} \times 10^{\circ}$	5	Specified
Ice age	$4^{\circ} \times 5^{\circ}$	5	Specified
Ice age	$8^{\circ} \times 10^{\circ}$	5	Specified

TABLE 2. Annual global average radiative properties.

(a) For 2CO ₂ experiments							
Quantity	2CO ₂ -M	Cont-M	Δ-M	2CO ₂ -F	Cont-F	Δ-F	Std. dev.-M
Surf air temp (°C)	18.4	14.3	4.1	18.6	14.3	4.3	0.1
Vert-int temp (°C)	-17.1	-21.0	3.9	-16.3	-20.3	4.0	0.1
Spec humidity (10 ⁻⁵)	338.0	255.4	32%	352.3	265.3	33%	0.8%
Rel humidity (%)	47.1	45.6	3%	46.2	44.4	4%	0.3%
High clouds (%)	29.0	29.3	-1%	22.0	25.8	-15%	0.5%
Medium clouds (%)	17.8	19.5	-9%	14.9	16.4	-9%	0.4%
Low clouds (%)	33.6	35.9	-6%	30.0	32.5	-8%	0.4%
Total clouds (%)	49.9	51.7	-3%	44.6	49.9	-11%	0.2%
Ground albedo (%)	11.0	11.9	-8%	10.4	11.3	-8%	0.5%
Planetary albedo (%)	28.8	30.2	-5%	26.5	28.2	-6%	0.3%
Abs surf S.W. (W m ⁻²)	176.3	173.4	2.9	182.2	178.3	3.9	0.3
Surf net L.W. (W m ⁻²)	-45.8	-50.0	4.2	-45.4	-49.7	4.3	0.2
Surf net rad (W m ⁻²)	130.5	123.4	7.1	136.9	128.6	8.3	0.3
Surf fluxes (W m ⁻²)	-124.6	-117.5	-7.1	-132.5	-124.3	-8.2	0.7
Surf net heat (W m ⁻²)	5.3	5.0	0.3	3.5	3.2	0.3	0.3
Net S.W. at top (W m ⁻²)	245.4	240.5	4.9	251.3	245.5	5.8	0.1
Net L.W. at top (W m ⁻²)	-237.5	-233.0	-4.5	-241.1	-235.8	-5.3	0.2
Net rad at top (W m ⁻²)	7.9	7.5	0.4	10.2	9.7	0.5	0.2

(b) For ice age expt							
Quantity	I.A.-M	Cont-M	Δ-M	I.A.-F	Cont-F	Δ-F	Std. dev.-F
Surf air temp (°C)	9.8	13.3	-3.5	9.5	13.3	-3.8	0.0
Vert-int temp (°C)	-24.0	-22.0	-2.0	-24.0	-21.5	-2.5	0.1
Spec humidity (10 ⁻⁵)	208.9	239.7	-13%	208.6	243.8	-14%	0.4%
Rel humidity (%)	43.7	45.1	-3%	42.5	43.9	-3%	0.1%
High clouds (%)	27.7	28.8	-4%	24.7	25.5	-3%	0.8%
Medium clouds (%)	20.4	19.8	3%	17.6	16.7	5%	0.9%
Low clouds (%)	37.7	36.5	3%	33.3	33.2	0%	0.3%
Total clouds (%)	51.7	51.7	0%	48.9	49.7	-2%	0.2%
Ground albedo (%)	15.8	11.7	35%	16.6	12.0	38%	0.1%
Planetary albedo (%)	32.0	30.1	6%	30.4	28.6	6%	0.1%
Abs surf S.W. (W m ⁻²)	167.2	172.5	-5.3	172.4	177.4	-5.0	0.1
Surf net L.W. (W m ⁻²)	-50.0	-50.5	0.5	-51.5	-51.0	-0.5	0.2
Surf net rad (W m ⁻²)	117.1	122.0	-4.9	120.9	126.4	-5.5	0.2
Surf fluxes (W m ⁻²)	-111.8	-115.5	3.7	-114.1	-120.5	6.4	0.7
Surf net heat (W m ⁻²)	3.9	5.5	-1.6	5.2	4.8	0.4	0.8
Net S.W. at top (W m ⁻²)	233.1	239.4	-6.3	238.0	244.0	-6.0	0.1
Net L.W. at top (W m ⁻²)	-226.7	-231.5	4.8	-228.4	-234.2	5.8	0.4
Net rad at top (W m ⁻²)	6.4	8.0	-1.6	9.6	9.9	-0.3	0.3

little cooling. The cooler climate sensitivity thus does appear to be resolution dependent. [Neither of the ice age experiments reported here used altered atmospheric CO₂. When CO₂ values were reduced 70 ppm, as implied by ice core data, surface air temperatures were changed by less than 1°C, due to the specification of sea surface temperatures, but the radiative imbalances increased by close to 2 W m⁻². Thus the ice age runs on both resolutions would have cooled by an additional 1–2°C, but again the total cooling would be less with the 4° × 5° model.]

The explanation for these results can be found in the components of the radiation balance (Table 2a, b). For the doubled CO₂ climate, the change in net shortwave radiation into the atmosphere (net S.W. at the top) exceeds the change in exiting longwave radiation (net L.W. at the top) by approximately the same

amount for both resolutions. The finer grid shortwave gain is greater due to its greater decrease in cloud cover, and the longwave loss is also greater, though temperature changes are similar, since the finer-grid control run was a warmer run. However, in the ice age experiments, there is no compensation: the increase in net longwave radiation is less in the medium-grid run, as the ice age surface and vertically integrated air temperature decreases are smaller in magnitude, while medium-grid shortwave radiation decreases somewhat more.

What accounts for the different responses in the warm and cold climates? The energy balance for the global, annual atmosphere is presented in Tables 3a, b. For the warm climate, the finer-resolution control run has greater evaporation, due primarily to stronger surface winds. Its hydrologic cycle is thus more active,

TABLE 3. Annual global average atmospheric energy balance.

(a) For 2CO ₂ expt							
Quantity	2CO ₂ -M	Cont-M	Δ-M	2CO ₂ -F	Cont-F	Δ-F	Std. dev.-M
Vert-int temp (°C)	-17.1	-21.0	3.9	-16.3	-20.3	4.0	0.1
Evaporation (mm d ⁻¹)	3.5	3.2	0.4	3.8	3.4	0.4	0.0
S.W. abs. by atm (W m ⁻²)	62.3	60.4	1.9	62.6	60.7	1.9	0.1
L.W. loss by atm (W m ⁻²)	-184.7	-176.0	-8.7	-189.3	-179.7	-9.6	0.3
Ht by L.S. cond (W m ⁻²)	7.6	7.9	-0.3	10.3	11.0	-0.7	0.1
Ht by m. conv. (W m ⁻²)	95.2	84.8	10.4	100.2	89.5	10.7	0.4
Sens ht flux (W m ⁻²)	22.4	25.7	-3.3	22.4	24.7	-2.3	0.2
Mc mass flx (10 ⁹ Kg s ⁻¹)	1809	1939	-6.7%	1687	1817	-7.2%	0.3%

(b) For ice age expt							
Quantity	I.A.-M	Cont-M	Δ-M	I.A.-F	Cont-F	Δ-F	Std. dev.-F
Vert-int temp (°C)	-24.0	-22.0	-2.0	-24.0	-21.5	-2.5	0.1
Evaporation (mm d ⁻¹)	2.9	3.1	-0.2	3.0	3.3	-0.3	0.0
S.W. abs. by atm (W m ⁻²)	58.8	60.0	-1.2	58.8	60.2	-1.4	0.1
L.W. loss by atm (W m ⁻²)	-169.5	-173.8	4.3	-170.0	-176.6	6.6	0.5
Ht by L.S. cond (W m ⁻²)	9.2	7.8	1.4	12.0	10.9	1.1	0.0
Ht by m. conv. (W m ⁻²)	76.8	82.6	-5.8	75.3	84.9	-9.6	0.5
Sens ht flux (W m ⁻²)	27.2	26.1	1.1	28.0	25.5	2.5	0.2
Mc mass flx (10 ⁹ Kg s ⁻¹)	1917	1963	-2.3%	1732	1815	-4.6%	0.1%

with greater latent heat release. This effect helps the atmosphere warm slightly relative to the medium grid. An equal increment to the temperature in both resolutions results in greater energy loss from the warmer finer-grid control, from the nonlinear dependence of thermal radiation on temperature. The compensatory effect on shortwave radiation, due to decreased cloud cover, will also be shown (below) to result from the warmer finer grid atmosphere, in association with its convective response. For the cold climates, the colder finer-grid ice age temperatures result from a greater decrease in heating by moist convection with this resolution.

The temperature change due to moist convection results from vertical motion, latent heat release, and reevaporation. In the control runs, moist convection produces warming at all levels, except for the lowest level in the medium grid resolution where reevaporative cooling dominates. The finer-grid control runs produce generally greater warming at high levels and less at lower levels (Fig. 1) (from both moist convection and large-scale rainfall), with its greater surface wind speeds, surface evaporation, precipitation, and penetrative convection. The resulting increased stabilization reduces the finer-grid convective mass flux (Table 3). (Note also that the convective parameterization moves one-half the grid box mass in each convective event, so less mass is moved in the finer grid each time.)

When CO₂ is doubled, the moist convective warming shifts to higher levels (Fig. 1), with less warming (and in fact cooling), below, as increased penetrative convection alters levels of latent heat release and reevaporation. The changes in the temperature profile are greater in the finer grid since slightly greater absolute

amounts of moisture are available; also the increased penetration extends one level higher up with this resolution. The finer-grid greater warming at high levels, and greater cooling at low levels, tend to balance, so the impact on overall atmospheric temperatures is relatively similar with the two resolutions (Table 3a), as is the reduced shallow and middle level convective mass flux arising from the increased stability.

In the ice age runs, the cooler surface temperatures inhibit convection, and convective mass flux again decreases in both experiments. There is reduced convective warming at all levels in both experiments. However, the finer-grid reductions are larger, as its evaporation decreases more (the stronger finer-grid winds amplify any surface flux change). There is no compensation of opposite tendencies at high and low altitudes, as with the warmer climate, and heating by moist convection is decreased substantially in the finer-grid ice age run. The finer-grid ice age atmosphere is thus cooler throughout, the longwave energy loss is less, and the finer-grid ice age experiment is in radiation balance without the necessity for additional surface cooling. Thus, the processes and parameterizations of convection and evaporation cause the climate sensitivity to be resolution dependent for the specific cold climate simulations, and not for the specific warmer climates in the GISS model; the latter result also depends on shortwave radiation and cloud cover, discussed next.

2) CLOUD COVER

Cloud cover parameterizations are very crude, and the cloud cover changes produced by the different

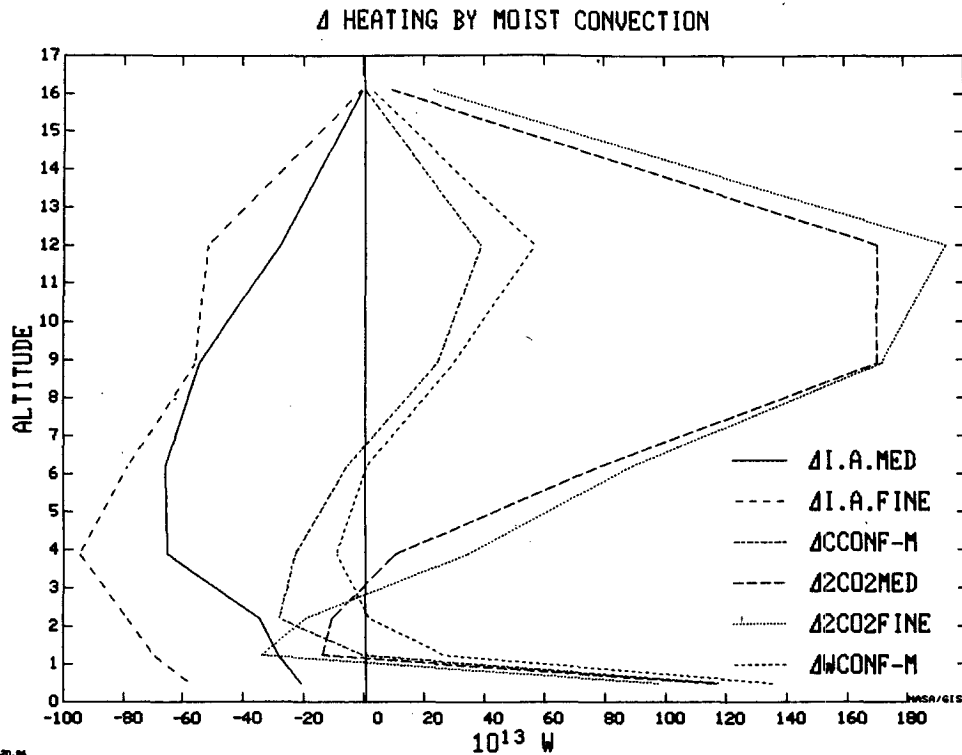


FIG. 1. Annual average change in heating by moist convection in the ice age and doubled- CO_2 experiments, on the finer and medium grid, compared to their respective control runs. Also shown is the difference in heating between the finer- and medium-grid control runs for the cold climate (CCON) and warm climate (WCON) experiments.

modeling efforts are all therefore uncertain. Nevertheless, the different general circulation models seem to produce generally similar cloud cover changes due to doubled CO_2 (Schlesinger and Mitchell 1987); Is this true of the different resolutions? The global average ice age cloud cover changes are relatively similar in the medium- and finer-grid experiments, but the doubled CO_2 changes are not (Table 2). The annual average cloud cover changes for the warmer climate are shown in Fig. 2. The finer-grid doubled CO_2 experiment produced large cloud cover decreases in the tropical upper troposphere, an effect greatly muted in the medium grid. The difference is associated with the cloud cover parameterization, and the degree of warming in the upper troposphere in the different simulations.

The cloud cover parameterization involves the calculation of the saturation humidity relative to water or to ice, depending upon the temperature. At temperatures colder than -40°C , saturation is relative to ice, an easier proposition than saturation relative to water. In sensitivity experiments, if this transition temperature is set to -60°C , model cirrus clouds are greatly diminished (Hansen et al. 1983). At temperatures between 0° and -40°C , saturation is calculated with respect to water, which will then subsequently freeze. The -40°C criterion is based on some experimental evidence, and is the value for homogeneous nucleation

(Wallace and Hobbs 1977), but the proper transition point and the sharpness of the transition are not well known.

The zonal average tropical upper troposphere temperatures (at 200 mb) warm from -48° to -39°C in the finer-grid doubled CO_2 experiment, which then requires that the test for supersaturation be conducted relative to water. This more severe condition results in the cloud cover decrease relative to the control run with this resolution. In the medium grid the temperature warms from -49° to -42°C at the same locations, which keeps the doubled CO_2 run in the regime of saturation with respect to ice. The cloud cover changes are thus small. The difference in the degree of warming is associated with the additional heating by moist convection (Fig. 1) in the finer-resolution model. Thus, the cloud cover change/resolution dependency is associated with the greater instability and convective penetration that can arise with finer resolution, in conjunction with the cloud generation formulation. In the ice age runs, temperatures are well below -40°C in both experiments, and the situation does not arise.

3) HIGH-LATITUDE TEMPERATURE AMPLIFICATION

The resolution dependency of the high-latitude temperature amplification, like the global sensitivity, can-

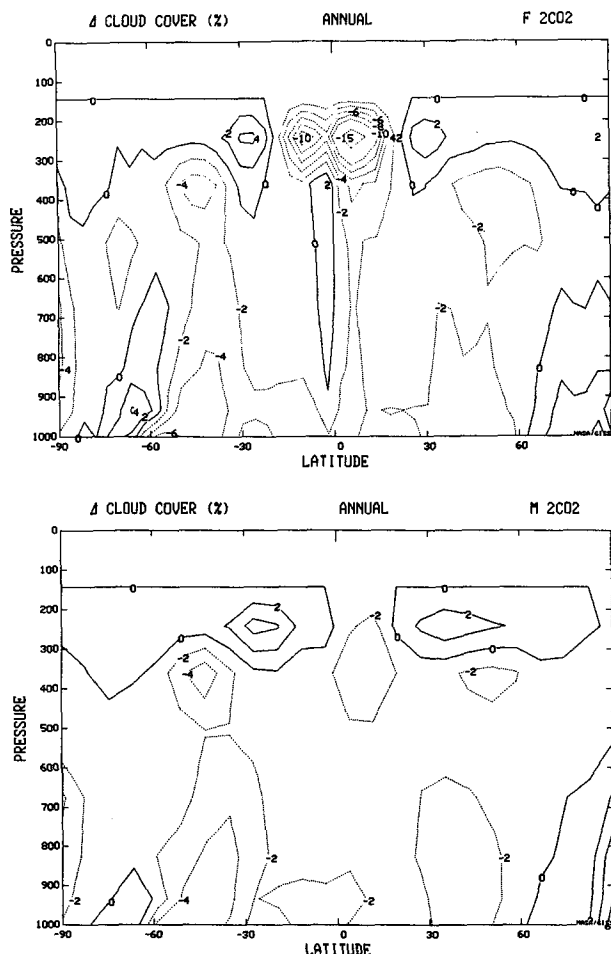


FIG. 2. Annual average change in cloud cover in the doubled- CO_2 experiments for the finer grid (top) and medium grid (bottom).

not be precisely defined with climate runs having specified sea surface temperatures, but an estimate of the different model tendencies can be obtained by considering the surface energy balance as a function of latitude. The medium-grid doubled CO_2 experiment produces an annual average surface air temperature increase of 6.6°C near 80°N , and 3.6°C near the equator, for a high-latitude amplification of 1.8. As discussed in detail elsewhere (Rind 1987b), this is considerably less than the high latitude amplification for the GFDL model. The finer-grid runs have temperature increases of 5.8°C and 3.8°C at high and low latitudes, respectively for an amplification of 1.5. However, this is achieved by specifying the sea surface temperature changes; What would the finer grid have done if the sea surface temperatures were allowed to adjust?

In the doubled CO_2 climate, the finer-grid model produces somewhat greater decreases in planetary albedo than does the medium grid (Fig. 3, top left). Not only does the finer-grid cloud cover decrease more at low latitudes, but at higher latitudes there is a greater

decrease in the ground albedo. The finer-resolution model has greater latitudinal delineation, so that as warming occurs, temperatures can exceed 0°C (and thus melt snow) in locations which, in the larger grid, remain below freezing. The planetary albedo change leads to greater excess solar radiation being absorbed at the surface (Fig. 3, middle left) at most latitudes. The change in net longwave radiation at the surface is relatively similar at most latitudes (Fig. 3, bottom left), since the change in atmospheric temperatures is similar, although the finer grid does have somewhat more longwave radiation at the surface due to its warmer temperatures and larger specific humidity increases at low latitudes associated with increased penetrative convection. (Note that the greater low-latitude increase in net longwave radiation occurs in the finer grid despite the greater decrease in high-level cloud cover.)

The finer-grid net radiation at the surface, the sum of the shortwave and longwave contributions, thus shows greater positive increases in the doubled CO_2 climate at most latitudes (Fig. 4, top left), with the largest increase in the tropics. Were this the only difference, one would expect low latitudes to initially warm in the finer grid, compared to the medium grid. However, the finer grid also has a much greater increase in surface fluxes of sensible and (especially) latent heat to the atmosphere (Fig. 4, middle left), due to the greater surface wind velocities which exist with this resolution. For a given difference between ground and surface air temperature or humidity, the greater wind speeds in the finer grid runs amplify the flux difference (the reason for these greater wind speeds is discussed below). The surface flux change offsets the radiation imbalance and produces a near-equatorial decrease in net surface heating (Fig. 4, bottom left), while at other latitudes the greater positive net radiation at the surface predominates. The initial tendency of the finer-grid doubled CO_2 run, therefore, is to cool the tropical waters, and warm other latitudes, relative to the effects generated with specified sea surface temperatures. What the final result would be cannot be determined, for if the tropical ocean waters were to cool, and reduce convection and atmospheric specific humidity, these influences would affect other latitudes and the global energy balance. Note that the medium grid doubled CO_2 experiment has little net heating at the surface, as it was run to equilibrium.

The ice age runs have 80°N /equatorial temperature changes of $-5.4/-1.6 = 3.4$ in the medium grid, and $-5.6/-1.4 = 4.0$ in the finer grid. Both ratios are higher than the model produced for the doubled CO_2 runs, and would therefore likely be reduced were the sea surface temperatures (and land ice) not specified. The ice age planetary albedo change is greater in the finer grid (Fig. 3, top right); in good part, this is the result of the increased resolution which allows some finer-resolution boxes to be below freezing that in the larger grid are parts of bigger, warmer boxes. This temperature dif-

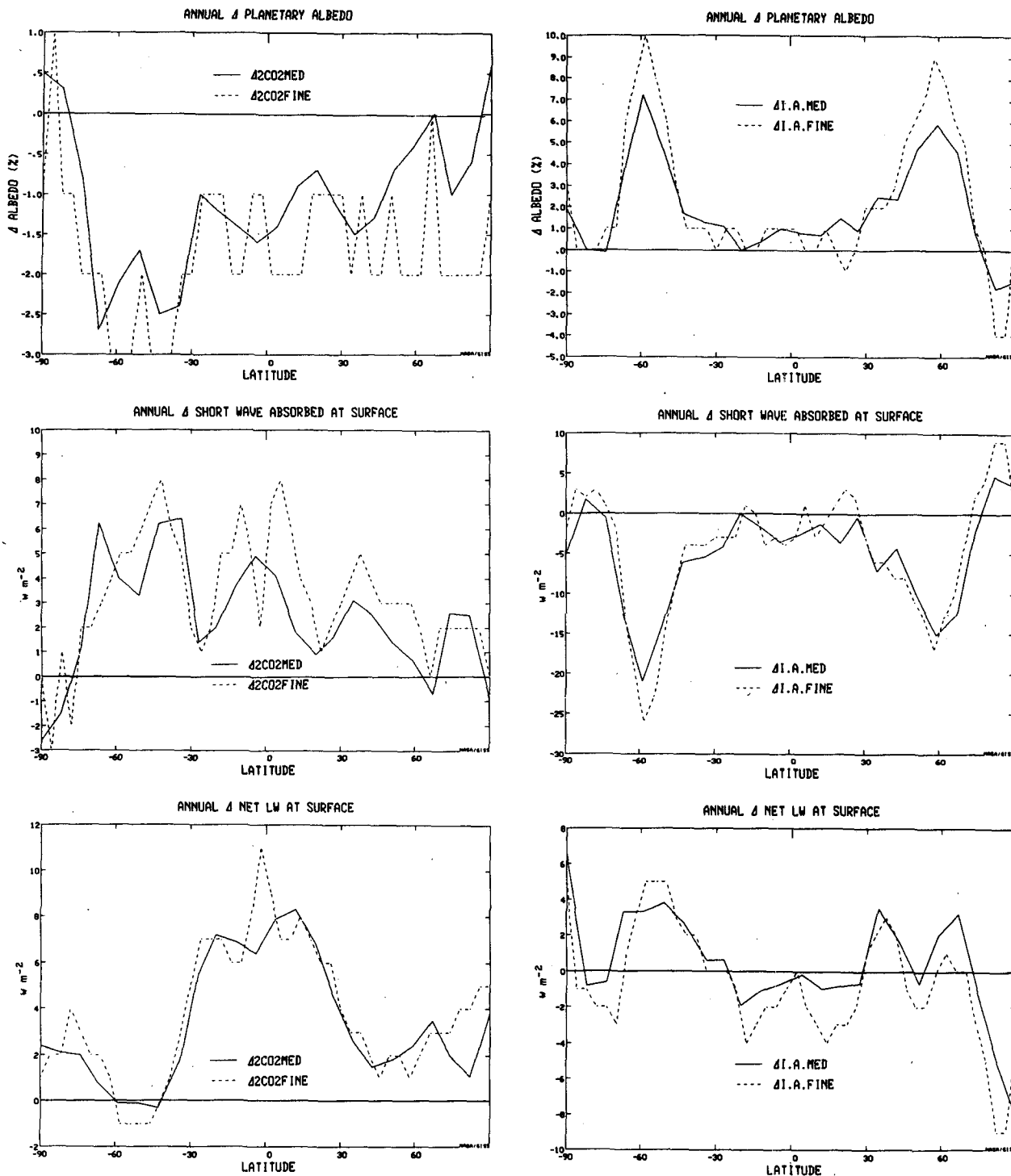


FIG. 3. Annual average changes for the doubled-CO₂ experiments (left) and ice age experiments (right) for planetary albedo (top), shortwave radiation absorbed at the surface (middle), and net longwave radiation at the surface (bottom). The solid line indicates the change between the medium grid experiment and control, while the dashed line represents the differences on the finer grid.

ference allows the finer-grid ice age run to have slightly more snow cover, especially in the marginal midlatitude regions where solar radiation is nonnegligible, and the resulting increased planetary albedo leads to slightly

greater reductions in shortwave radiation at the surface (Fig. 3, middle right) at these latitudes. As discussed above, the finer-grid ice age atmosphere shows greater temperature decreases due to greater decreases in con-

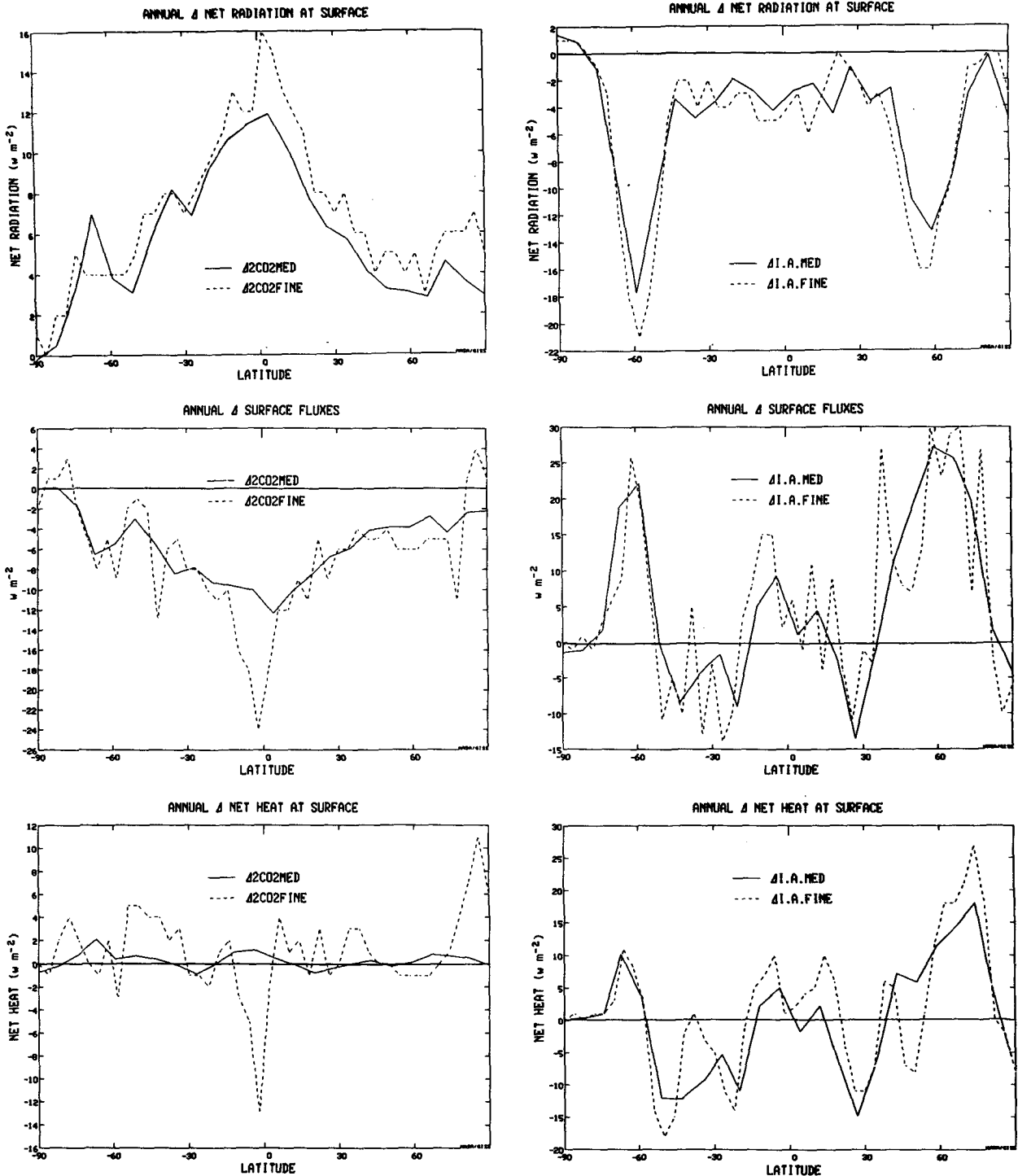


FIG. 4. As in Fig. 3 but for net radiation at the surface (top), surface fluxes of latent and sensible heat (middle), and net heating at the surface (bottom).

vective heating, and so experiences a greater decrease in net longwave radiation at the surface (Fig. 3, bottom right).

With both reduced shortwave and longwave energy fluxes at the surface relative to the medium grid

changes, the net radiation change at the surface is more negative at tropical and midlatitudes in the finer grid (Fig. 4, top right). This effect is overwhelmed by the change in the surface fluxes (Fig. 4, middle right), which provide a positive source of heat for the surface through

reduced evaporation. The reduction is again somewhat larger in the finer grid, as the stronger surface winds magnify any change; in addition, the finer-grid model atmosphere, being slightly colder, can hold less moisture. Thus, there is relatively less evaporation in the tropical finer-grid ice age experiment, and the net heating at the surface is more positive in this region in the finer grid (Fig. 4, bottom right). At high northern latitudes, the increased sea ice prevents ocean surface fluxes in both resolutions, and the greater wind speeds in the finer grid exaggerate the effect. The increased heating which the finer-grid ice age experiment experiences at both high and low latitudes would limit any appreciable change in high-latitude amplification as a function of resolution. Note that both models would substantially reduce the high-latitude amplification if the boundary conditions were not specified, an expected result given the smaller amplification characteristic of the equilibrium run for doubled CO_2 .

b. Atmospheric dynamics

1) MEAN MERIDIONAL CELLS

Given the distinctive surface flux changes in these experiments, it might be supposed that differences would appear in the Hadley cell simulations. The control run December–February streamfunction, and changes due to the doubled CO_2 and ice age climates are shown in Fig. 5 for both resolutions. The finer-grid control run (Fig. 5, top left) produces a better defined Ferrel cell (more realistic), and a Hadley cell with less direct extension across the equator [which, from the analysis of Oort and Rasmusson (1971) is less realistic]. The doubled CO_2 experiment in the finer grid shows strong increases in the low-latitude Hadley cell intensity, and decreases in the subtropical Hadley cell and in the lower midlatitude Ferrel cell (Fig. 5, middle left), effects which are missing in the medium grid experiment (Fig. 5, middle right). The ice age experiments have increased Hadley cell intensities for both resolutions (Fig. 5, bottom), but only the finer grid shows a substantially greater Ferrel cell at upper midlatitudes.

To understand the reasons for these differences, the December–February energy balances for the vertically integrated atmosphere at latitude bands 4° and 8° wide (for the respective resolutions) centered at 2° – 4°S and 50° – 51°N are given in Tables 4a,b. The mean vertical velocities which contribute to the meridional cells are also shown; since the temperature change over the three month time period is negligible, these vertical motions can be thought of as the resultant of energy imbalances generated by the other heating or cooling terms, although all processes actually operate interactively.

Focusing first on the low-latitude balance, the major differences between the medium- and finer-grid control runs are that the finer grid has more longwave energy loss and less moist convective heating. The greater

longwave energy loss is simply an expression of the fact that the finer grid is a warmer run overall (Table 2), as discussed above. The reduced moist convective heating is peculiar to this latitude. It arises in response to the greater precipitation and latent heat release north of the equator in the finer grid (a model deficiency), shown in Fig. 6 (top). Where the model rains easily in the medium grid, it tends to rain even more in the finer grid, inducing local meridional cells. The downdrafts of these cells make other regions drier in the finer grid, the effect seen at 2°S . The greater downward velocity (or reduced upward velocity) at this latitude warms the finer grid control run relative to the medium grid, balancing (and producing) the increased longwave radiative loss and reduced moist convective latent heat release.

The finer-grid doubled CO_2 experiment shows strong increases in upward vertical velocity at this latitude, indicative of the increased equatorial Hadley cell (Fig. 5). This is the interactive response to the much larger increase in moist convective heat release in this experiment (Fig. 6, middle). Again, the same principle discussed for the relative control runs applies; where moist convective rainfall, or rainfall changes, occur in the medium grid, the effect is amplified in the finer grid. Even the ice age experiments show a similar tendency, with a strong increase in moist convective heating and vertical motion in the finer grid experiment (Fig. 6, bottom), although here the differences with the medium grid are not as large. The resolution dependency of the Hadley cell response in the warmer climates is thus related to the hydrologic cycle/convective sensitivity to grid size.

At 50°N (Table 4b), the finer-grid control run has much stronger upward vertical velocities, indicative of its stronger Ferrel cell. The increased vertical motion provides cooling to balance increased latent heat release from greater precipitation, and increased eddy sensible heat convergence. Slight changes with resolution occur in doubled CO_2 experiments, only occasionally significant, as the increased relative subsidence and moist convective heat release balance increased thermal loss, and reduced sensible heat fluxes and eddy heat convergence on both spatial scales. However, for the ice ages, the finer-grid experiment shows much stronger downward vertical velocity relative to the control. The finer-grid ice age run has a colder atmosphere, relative to the medium grid, and thus much less longwave energy loss. The stronger surface wind velocities in the finer grid cause the sensible heat flux terms to increase more than in the medium grid. But the difference in vertical velocity response appears to be most affected by the change in eddy heat convergence, with the ice age finer-grid loss producing less heating; its vertical velocity is thus downward to provide the lost positive temperature tendency. Results for this latitude, and the Ferrel cell, in general, emphasize the importance of changes in eddy properties.

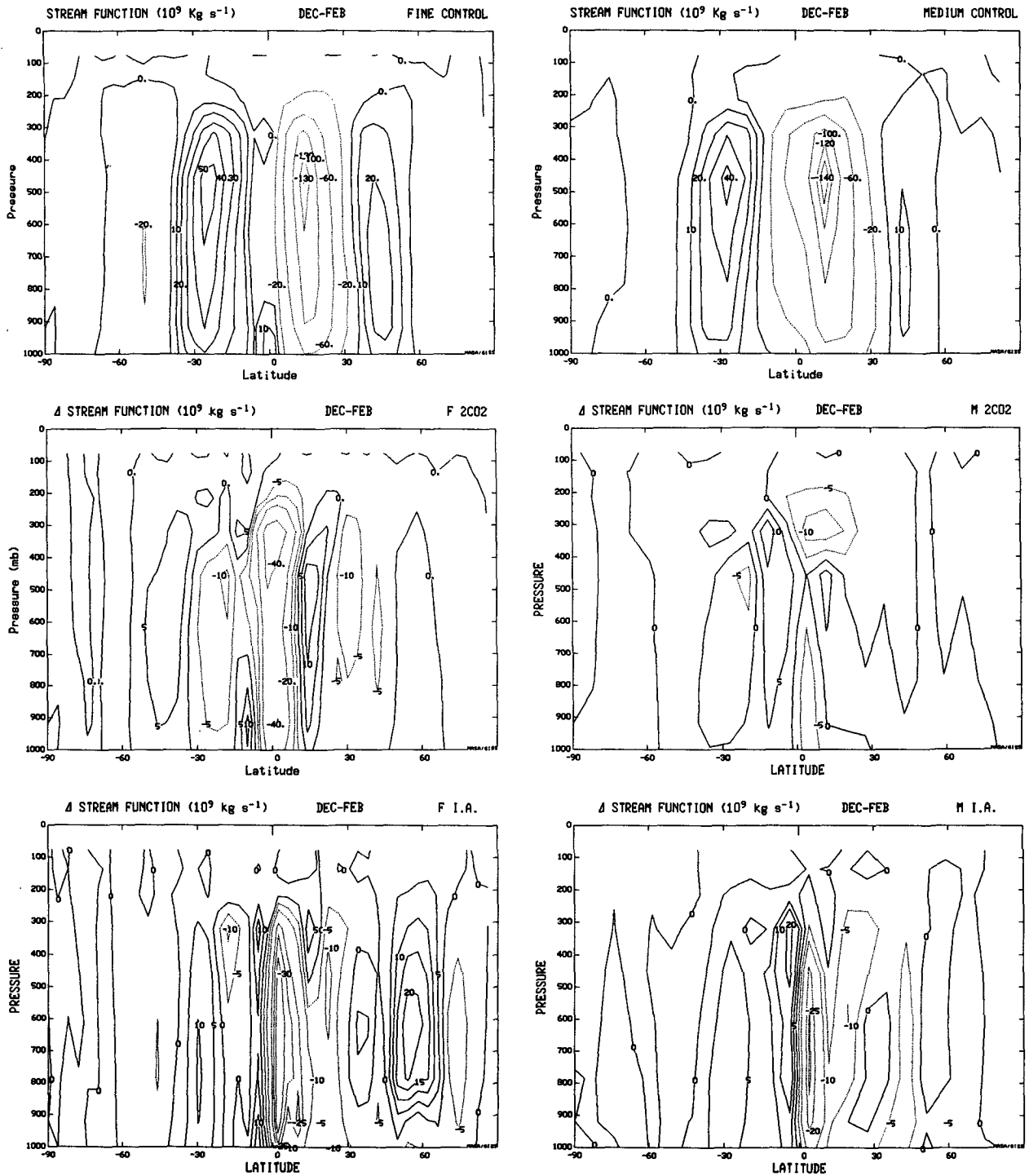


FIG. 5. Finer-grid (left) and medium-grid (right) results for December–February control run streamfunction (top), change in streamfunction in the doubled- CO_2 climate (middle) and in the ice age climate (bottom). Control run values in this and other figures are for the cold climate control runs (CCON).

2) EDDY ENERGY

The energetics of the different resolution models, and their changes in the warm and cold climates, are

presented in Tables 5a,b. The finer-grid model has much less eddy kinetic energy, and much more zonal kinetic energy than the medium grid. The changes in the energy partitioning and energy cycle in the warm

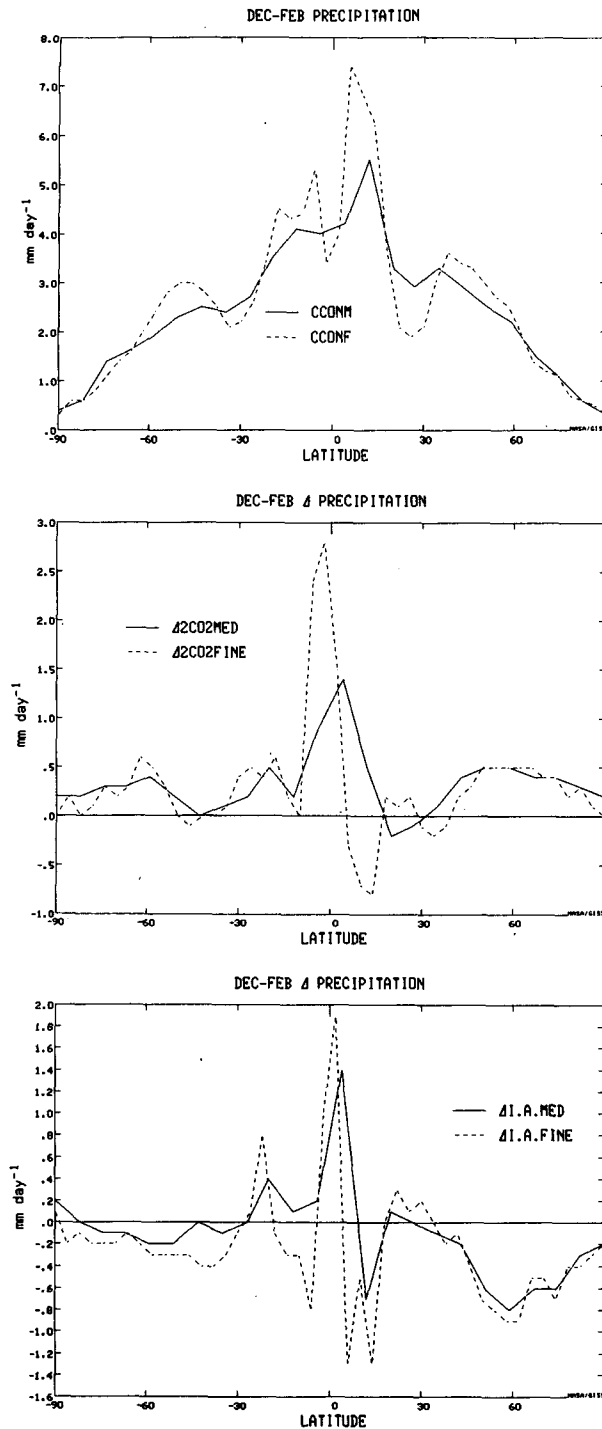


FIG. 6. December–February precipitation in the medium-grid (solid) and finer-grid (dashed) control runs (top), and change in precipitation in the doubled- CO_2 climate (middle) and ice age climate (bottom).

and cold climates show some resolution dependency, but the effects are generally of the same sign and order of magnitude. There is a tendency for the absolute

amount of change in energy quantities to be similar for the different resolutions, so the percentage changes are larger in the resolution with smaller control run values, e.g., the medium-grid doubled CO_2 run has about twice the percentage increase in zonal kinetic energy as the finer grid, while the fine-grid ice age run has about twice the increase in eddy kinetic energy.

The differing amounts of eddy and zonal kinetic energy in the two resolutions are indicative of fundamental differences in how model energy transfers occur. Shown in Fig. 7 are the energy spectra for the control runs, for total eddy energy (top), standing eddy energy (defined for the seasonal time scale) (middle), and transient eddy energy (bottom). The finer-grid reduction in eddy energy occurs primarily in the intermediate wavenumber scale, especially for transient eddies. There is larger finer-grid longwave energy in the stationary component, but less in the transient mode.

The energy budgets for the zonal mean kinetic energy (wavenumber 0), the long waves (wavenumbers 1–5), and intermediate waves (wavenumbers 6–10) are given in Table 6, along with the changes in the different climate experiments. The kinetic energy production and destruction terms closely balance over the 3 month period, indicating that there is little net kinetic energy difference between November and March. The generation of kinetic energy by the pressure gradient force is basically a potential energy to kinetic energy transfer, with a small residual representing energy flux into the stratosphere; this baroclinic transfer is much stronger in the finer-grid control run for the long waves, but the additional energy is lost via transfer of energy nonlinearly to other wavenumbers and, especially, to the zonal mean flow. The energy flux result is consistent with the model experiments of Hayashi and Golder (1987), which indicated that in the mature stage, ultralong transient waves lose energy via nonlinear interaction when transfer to the zonal mean flow is included; as shown in Fig. 7, it is the transient longwave energy which is less with the finer resolution.

For the intermediate-scale wavenumbers, there is little difference in baroclinicity between the finer and medium grids, but again the finer grid loses energy due to nonlinear transfers. There is less direct generation of zonal mean kinetic energy from potential energy in the finer grid (as its Ferrel cell is stronger), but this is more than compensated for by the large nonlinear transfer of energy into zonal kinetic energy by eddies. Energy loss by convective mixing of momentum is somewhat larger in the medium grid, due to its greater convective mass flux (the finer grid, again, has greater penetrating convection and atmospheric stabilization), while there is greater loss of energy due to surface friction in the finer grid as surface winds are stronger.

The resultant picture is one of a resolution difference in zonal and eddy kinetic energy, and in the kinetic energy spectrum, strongly associated with the different nonlinear energy transfers. The nonlinear term in the

TABLE 4. Dec-Feb tropospheric thermal balance.

(a) At 2-4°S (Units °d ⁻¹)							
Climate run	Vertical velocity (10 ⁻⁵ mb ⁻¹)	Solar heating	Thermal cooling	Moist convective heating	Sensible heat flux	Eddy convection	Mean cell subsidence heating
Wcon-M	5	0.67	-1.55	1.08	0.15	0.00	-0.35
2CO ₂ -M	6	0.70	-1.64	1.29	0.12	-0.04	-0.51
Wcon-F	0	0.67	-1.64	0.99	0.10	-0.07	-0.05
2CO ₂ -F	11	0.69	-1.74	1.71	0.08	-0.16	-0.90
Ccon-M	5	0.67	-1.53	1.05	0.17	0.05	-0.31
I.A.-M	5	0.66	-1.53	1.03	0.14	-0.02	-0.32
Ccon-F	-2	0.66	-1.61	0.84	0.12	0.09	0.08
I.A.-F	5	0.65	-1.53	1.10	0.10	-0.03	-0.35
St. dev.-M	2.10	0.00	0.02	0.10	0.01	0.00	0.13
St. dev.-F	0.90	0.00	0.01	0.03	0.00	0.00	0.04

(b) At 50°N (Units °d ⁻¹)									
Climate run	Vertical velocity	Solar heating	Thermal cooling	M.C. heat	L.S. cond	Sensible heat flux	Eddy convection	Mean subsidence	Mean convection
Wcon-M	2	0.18	-1.37	0.43	0.24	0.16	0.36	-0.14	-0.02
2CO ₂ -M	2	0.18	-1.44	0.53	0.25	0.13	0.31	-0.09	-0.19
Wcon-F	5	0.19	-1.38	0.48	0.31	0.17	0.38	-0.32	0.00
2CO ₂ -F	4	0.19	-1.44	0.59	0.31	0.15	0.30	-0.16	-0.13
Ccon-M	1	0.17	-1.36	0.42	0.23	0.17	0.32	-0.04	0.00
I.A.-M	-1	0.16	-1.30	0.24	0.29	0.19	0.25	0.22	0.00
Ccon-F	4	0.18	-1.37	0.47	0.31	0.17	0.38	-0.27	0.00
I.A.-F	-2	0.16	-1.23	0.28	0.35	0.31	-0.07	0.26	-0.13
St. dev.-M	1.30	0.00	0.01	0.02	0.01	0.01	N.A.*	0.05	N.A.
St. dev.-F	1.30	0.00	0.01	0.02	0.01	0.01	N.A.	0.09	N.A.

* N.A. indicates values not available.

equation of motion, which is responsible for these transfers, is more accurately approximated in the finer grid, as the numerical finite difference is closer to the true derivative on the finer scale, while the magnitude of the nonlinear interactions is larger as local wind gradients are better resolved.

How does model resolution affect the generated spectrum and energy transfers in the climate experiments? In the doubled CO₂ experiment, both resolutions gain zonal kinetic energy via greater nonlinear energy transfer (Table 6b; it is also indicated by the greater barotropic energy transfer in Table 5). Both resolutions suffer losses in longwave energy due to nonlinear energy transfers, and in intermediate-scale energy due to decreased baroclinic generation. However, the greatest energy loss in the finer grid occurs in the longest wavenumbers and is mostly in the standing wave component, while the greatest energy loss in the medium grid occurs in the medium-scale waves, mostly in the transient component. Thus, energy is preferentially lost in the component and length scale in which it is most abundant in the respective resolutions.

In the ice age experiments, energy is gained at all wavenumbers, in both resolutions. The finer grid has greater longwave increases, while the medium grid has more intermediate-scale energy increase than does the finer grid, again mimicking the control runs. Both

standing and transient eddy energy increases occur through the greater part of the spectrum, but the excess longwave energy change in the finer grid is basically stationary wave energy. This increase arises due to increased baroclinic generation, associated presumably with the better defined ice age topography on the finer resolution; it is balanced by nonlinear energy transfer into the zonal mean flow, so that while barotropic energy transfer and the zonal kinetic energy increase in both resolutions, the change is greater in the finer grid. In both the cold and warm climates, on both resolutions, increased nonlinear energy transfer to the zonal mean flow occurs regardless of the sign of the eddy energy change. Reasons for this result, and the consequences of the different zonal mean flow structures, are discussed in section 3.

3) ZONAL MEAN WIND AND EDDY ENERGY FLOW

The zonal wind fields for December-February are presented in Fig. 8. Zonal winds are stronger in the finer-grid control at middle latitudes (Fig. 8, top) due to greater energy transfer from eddies (Tables 5, 6). At low latitudes, the east winds are also greater in the finer grid; this is partly a result of greater eddy forcing here as well, but more important is the diminished moist convective mixing of momentum. Momentum mixing

TABLE 5. Northern Hemisphere Dec–Feb dynamical quantities.

(a) For 2CO ₂ experiments							
Quantity	2CO ₂ -M	Cont-M	Δ-M	2CO ₂ -F	Cont-F	Δ-F	Std. dev.-M
Precip (mm d ⁻¹)	3.7	3.3	12%	3.9	3.7	5%	3%
Hadley c pk (10 ⁹ Kg s ⁻¹)	-134	-136	-1%	-135	129	5%	3%
H.C. extent (N. Lat)	42.0	41.3	0.7	38.8	37.8	1.0	N.A.
Ferrel c pk (10 ⁹ Kg s ⁻¹)	10	12	-17%	29	32	-9%	36%
U (m s ⁻¹) (32°N, 200 mb)	39.6	34.7	14%	47.9	45.6	5%	4%
Stat eke (10 ⁴ J m ⁻²)	37.8	38.4	-2%	20.5	22.8	-10%	5%
Trans eke (10 ⁴ J m ⁻²)	84.5	92.9	-9%	73.1	79.1	-8%	N.A.
Eddy N.TR.S.H. (10 ¹⁴ W)	14.8	16.1	-8%	15.2	17.1	-11%	4%
Eddy N.TR.L.H. (10 ¹⁴ W)	16.4	13.7	20%	15.5	13.7	12%	4%
Eddy N.TR.S.E. (10 ¹⁴ W)	31.0	29.7	4%	30.1	30.2	0%	4%
Atm N.TR.S.E. (10 ¹⁴ W)	47.1	44.1	7%	47.9	45.1	6%	4%
ST.E. N.TR. mom (10 ¹⁸ J)	6.5	6.1	7%	7.8	9.6	-19%	24%
TR.E. N.TR. mom (10 ¹⁸ J)	3.4	2.4	42%	8.0	6.9	16%	N.A.
Zonal K.E. (10 ¹⁷ J)	1757	1574	12%	2276	2159	5%	4%
Eddy K.E. (10 ¹⁷ J)	2693	2904	-7%	2098	2278	-8%	2%
Zonal A.P.E. (10 ¹⁷ J)	13067	13308	-2%	14355	14896	-4%	3%
Eddy A.P.E. (10 ¹⁷ J)	4934	5529	-11%	5268	5841	-10%	2%
EAPE→EKE (10 ¹² W)	452	484	-7%	663	686	-3%	5%
ZAPE→ZKE (10 ¹² W)	170	171	-1%	65	67	-3%	14%
EKE→ZKE (10 ¹² W)	37	30	23%	180	173	4%	N.A.
DKZ (10 ¹² W)	199	194	3%	240	236	2%	N.A.
DKE (10 ¹² W)	407	452	-10%	456	498	-8%	N.A.
GAZ (10 ¹² W)	1261	1442	-13%	1256	1554	-19%	N.A.
GAE (10 ¹² W)	333	442	-25%	298	352	-15%	N.A.

(b) For ice age experiments							
Quantity	I.A.-M	Cont-M	Δ-M	I.A.-F	Cont-F	Δ-F	Std.dev.-F
Precip (mm d ⁻¹)	3.1	3.2	-3%	3.3	3.5	-6%	1%
Hadley c pk (10 ⁹ Kg s ⁻¹)	-141	-132	7%	-129	-131	-2%	3%
H.C. extent (N. Lat)	44.7	42.6	2.1	36.0	36.3	-0.3	N.A.
Ferrel c pk (10 ⁹ Kg s ⁻¹)	8	10	-20%	36	28	29%	20%
U (m s ⁻¹) (32°N, 200 mb)	34.6	33.4	4%	37.6	41.6	-10%	4%
Stat eke (10 ⁴ J m ⁻²)	25.8	19.2	34%	37.5	20.6	82%	5%
Trans eke (10 ⁴ J m ⁻²)	132.9	113.8	14%	87.9	77.4	14%	N.A.
Eddy N.TR.S.H. (10 ¹⁴ W)	21.5	16.6	30%	22.4	16.1	39%	5%
Eddy N.TR.L.H. (10 ¹⁴ W)	14.0	13.1	7%	13.1	12.0	9%	2%
Eddy N.TR.S.E. (10 ¹⁴ W)	35.1	29.6	19%	35.0	27.5	27%	4%
Atm N.TR.S.E. (10 ¹⁴ W)	48.9	42.3	16%	47.8	40.6	18%	3%
ST.E. N.TR. mom (10 ¹⁸ J)	5.5	5.6	-2%	14.7	7.2	104%	13%
TR.E. N.TR. mom (10 ¹⁸ J)	6.4	3.7	73%	8.0	8.8	-9%	N.A.
Zonal K.E. (10 ¹⁷ J)	1654	1539	7%	2052	1905	8%	2%
Eddy K.E. (10 ¹⁷ J)	3505	2936	19%	2874	2208	30%	2%
Zonal A.P.E. (10 ¹⁷ J)	20075	13045	54%	22489	14198	58%	2%
Eddy A.P.E. (10 ¹⁷ J)	9221	5680	62%	9193	6071	51%	1%
EAPE→EKE (10 ¹² W)	737	492	50%	1006	697	44%	4%
ZAPE→ZKE (10 ¹² W)	38	163	-77%	-146	19	-868%	139%
EKE→ZKE (10 ¹² W)	172	30	473%	377	197	91%	N.A.
DKZ (10 ¹² W)	206	188	10%	225	210	7%	N.A.
DKE (10 ¹² W)	555	451	23%	616	490	26%	N.A.
GAZ (10 ¹² W)	2344	1454	61%	2305	1500	54%	N.A.
GAE (10 ¹² W)	591	428	38%	528	325	62%	N.A.

smooths the wind profile so it reduces kinetic energy throughout, and, as noted previously, the finer grid has less overall moist convection (Table 3) due to the greater penetration and over stabilization which results when convection does occur.

The different zonal wind structures in the two resolutions interact with the different eddy energies to

produce a consistent picture of the alteration in eddy forcing of the zonal mean flow. The control run Eliassen–Palm (EP) vertical and northward fluxes and divergences for both resolutions, are presented in Fig. 9. The medium grid, with greater eddy energy, has a greater vertical energy flux (normalized by the zonal wind) at midlatitudes (Fig. 9, top); it also has a greater

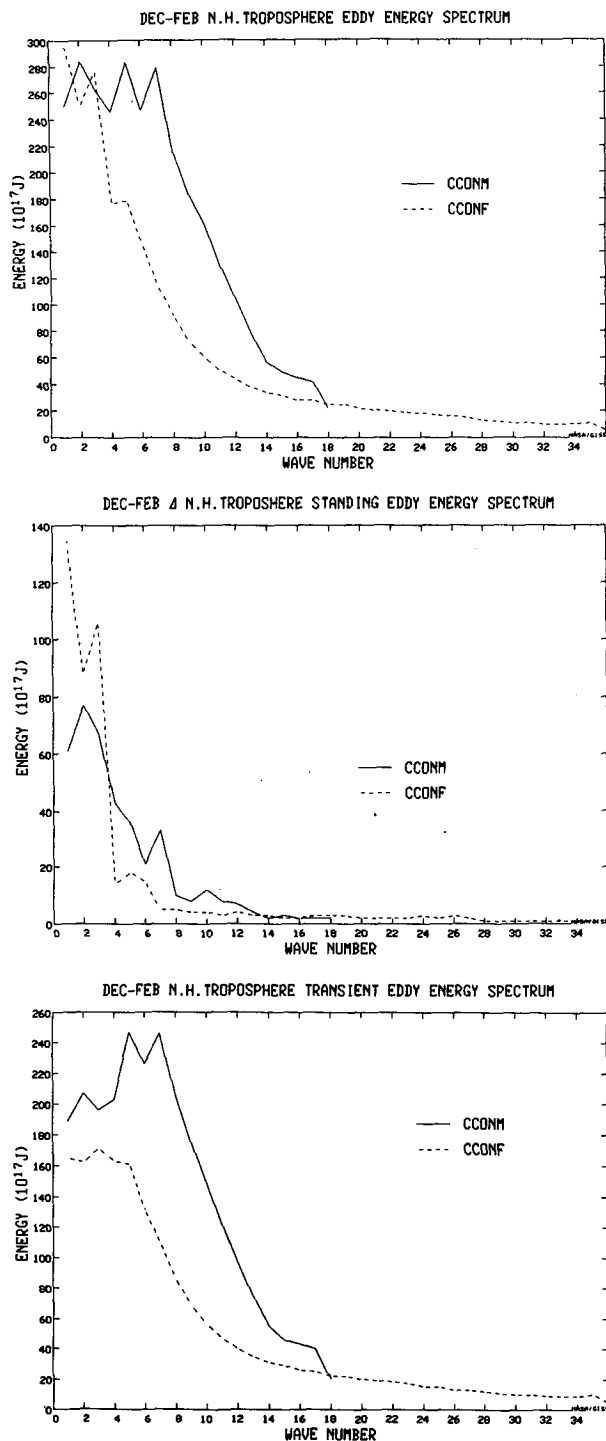


FIG. 7. Medium-grid (solid) and finer-grid (dashed) control run values of the December-February eddy energy spectrum (top), standing eddy energy spectrum (middle), and transient eddy energy spectrum (bottom).

vertical flux from 10° to 30°N , as the stronger east winds in the finer grid at these latitudes limit vertical energy propagation. This low-latitude vertically prop-

agating energy in the medium grid (only) turns northward (Fig. 9, middle); it is responsible for EP flux divergences north of the equator, and strong subtropical convergences, while the finer grid has reduced values for both of these effects (Fig. 9, bottom). As EP flux divergences/convergences generate west/east winds, the greater divergence/convergence pattern in the medium grid broadens the westerlies equatorward, but weakens their magnitude, consistent with the zonal wind structures (Fig. 8).

The discussion thus becomes circular, with the different wind structures used to explain the different eddy energy propagation patterns, and the EP flux divergences responsible in part for the wind structures. The effect most likely begins with the resolution dependence of convection at low latitudes, and its effect, through momentum mixing, on the subtropical zonal flow. Another possibility is the solution for the nonlinear term in the equation of motion. Physically this term translates, in perturbation notation, into eddy momentum transports. The finer grid should be providing a more accurate finite difference calculation of this quantity, and the magnitude of the momentum transport in the jet stream region is more in accord with observations for the finer resolution, (e.g., Oort and Rasmusson 1971). However, the finer grid control run has northward eddy momentum transport everywhere north of the equator in this season (consistent with the southward EP flux), in contrast to observations which indicate that the eddy transport of momentum should be southward in the region just north of the equator, more like the medium-grid pattern. The east winds in the finer-grid upper troposphere appear to extend too far poleward in the subtropics, with an accurate location for the zero wind line occurring between the location of the two model resolution results (e.g., Oort 1983). Both the convective mixing by momentum or the convection scheme itself, and the numerical calculation of the nonlinear effect, appear to work together to generate this discrepancy. The nonlinear transfers, which operate on the existing kinetic energy, may also be influenced by the magnitude of dissipation in the model, a subject returned to in section 4.

The changes in wind velocity for the different resolution climate experiments are shown in Fig. 8 (middle, bottom). The energy loss in the 2CO_2 runs produces decreased upward energy propagation at both mid- and subtropical latitudes in the medium-grid run, while the effect is confined more to midlatitudes in the finer grid, (since there was little at low latitudes in the finer grid control). The tropical/subtropical divergence/convergence pattern is thus weakened in the medium-grid doubled CO_2 run, while only the convergence pattern is weakened in the finer grid. So the subtropical jet stream is strengthened in both resolutions, while the medium grid has stronger upper troposphere tropical easterlies.

The energy increase in the ice age runs produces

TABLE 6(a). Northern Hemisphere Dec–Feb kinetic energy balance (Units 10^4 J m^{-2} (energy), W m^{-2} for rates). Observations from Saltzman (1970).

Climate run/observed	Wave number	Kinetic energy	Nonlinear transfer	Pressure gradient	Convective momentum mixing	Surface friction
CCON-M	0	60.5	0.12	0.64	-0.54	-0.20
	1–5	10.4	-0.06	0.22	-0.07	-0.09
	6–10	8.5	0.01	0.13	-0.06	-0.08
CCON-F	0	74.6	0.77	0.07	-0.39	-0.44
	1–5	9.3	-0.17	0.36	-0.06	-0.13
	6–10	3.8	-0.03	0.13	-0.03	-0.06
Observed	0	100.0	0.48	0.00	-0.48	net
	1–5	18.6	-0.02	0.27	-0.25	dissipation
	6–10	8.0	-0.09	0.30	-0.21	

(b) Northern Hemisphere Dec–Feb kinetic energy balance change (Units 10^{17} J , 10^{12} W).

Climate change	Wave number	Kinetic energy	Nonlinear transfer	Pressure gradient	Convective momentum mixing	Surface friction
$\Delta 2\text{CO}_2\text{-M}$	0	183	7	-1	0	-5
	1–5	-3	-5	3	1	1
	6–10	-23	3	-7	2	2
$\Delta 2\text{CO}_2\text{-F}$	0	117	7	-2	-9	5
	1–5	-17	-4	-1	1	2
	6–10	-10	0	-3	1	1
$\Delta \text{I.A.-M}$	0	115	142	-125	5	-23
	1–5	70	-23	39	-3	-11
	6–10	28	-6	9	0	-4
$\Delta \text{I.A.-F}$	0	147	180	-165	0	-15
	1–5	107	-44	64	-2	-16
	6–10	19	8	-3	0	-4

increased upward vertical fluxes over the same wider range of latitudes in the medium grid experiment. Both resolution ice age experiments produce more eddy deceleration in the jet stream region. However, the medium-grid run has an increase in upper tropospheric wind velocity at 30°N while the finer grid shows a decrease (Fig. 8), amongst many other differences. The momentum balance for the region indicates that in the medium-grid run, the Coriolis force acting on an increased meridional wind more than offsets the eddy energy deceleration, while in the finer grid, the meridional wind increase is less, and deceleration thus dominates. The difference can be related to the altered mean circulation cells (Fig. 5), with the finer grid experiencing a much stronger increase in the Ferrel cell. As indicated in Table 4, that difference occurs because of an alteration in the eddy heat transport convergence.

The results show that the eddy energy reacts with differing spectral characteristics in the different resolution experiments (Table 6b); we now need to investigate how the energy transports differ. Note that the different response of the Ferrel cell with resolution alters the zonal wind pattern and thus the EP flux pattern at mid- and high latitudes; for example, in the finer grid, the excess eddy energy preferentially flows to higher latitudes than in the medium grid. This further alters the EP flux divergence pattern, the eddy forcing of the zonal mean wind, and the mean wind itself.

4) ENERGY TRANSPORTS

Although the finer grid has less eddy energy than the medium grid, the eddy transports of heat and moisture are very similar (Hansen et al. 1983). However, resolution-dependent differences in eddy energy in the climate change experiments do lead to differences in eddy transports. The vertically integrated change in eddy kinetic energy, eddy northward sensible heat flux, and latent heat flux for the different resolutions are shown in Fig. 10. The finer-grid ice age run has more eddy energy at upper midlatitudes (Fig. 10, top right), and greater sensible heat transport there (Fig. 10, middle right). The eddy energy increase arises from the greater generation of standing long waves, as indicated in Table 6b. In the doubled CO_2 experiments, the finer grid experiences a greater reduction in midlatitude eddy energy (Fig. 10, top left), again associated with a greater reduction in baroclinic generation of standing long waves (Tables 5, 6), and a greater reduction in northward sensible heat transport at these latitudes (Fig. 10, middle left).

The ice-age eddy latent heat transport change (Fig. 10, bottom right) is relatively similar in the two resolutions, with increased transport associated with the larger eddy energy in the subtropics and lower midlatitudes. At higher latitudes, decreased transport occurs due to the colder atmosphere and reduced absolute

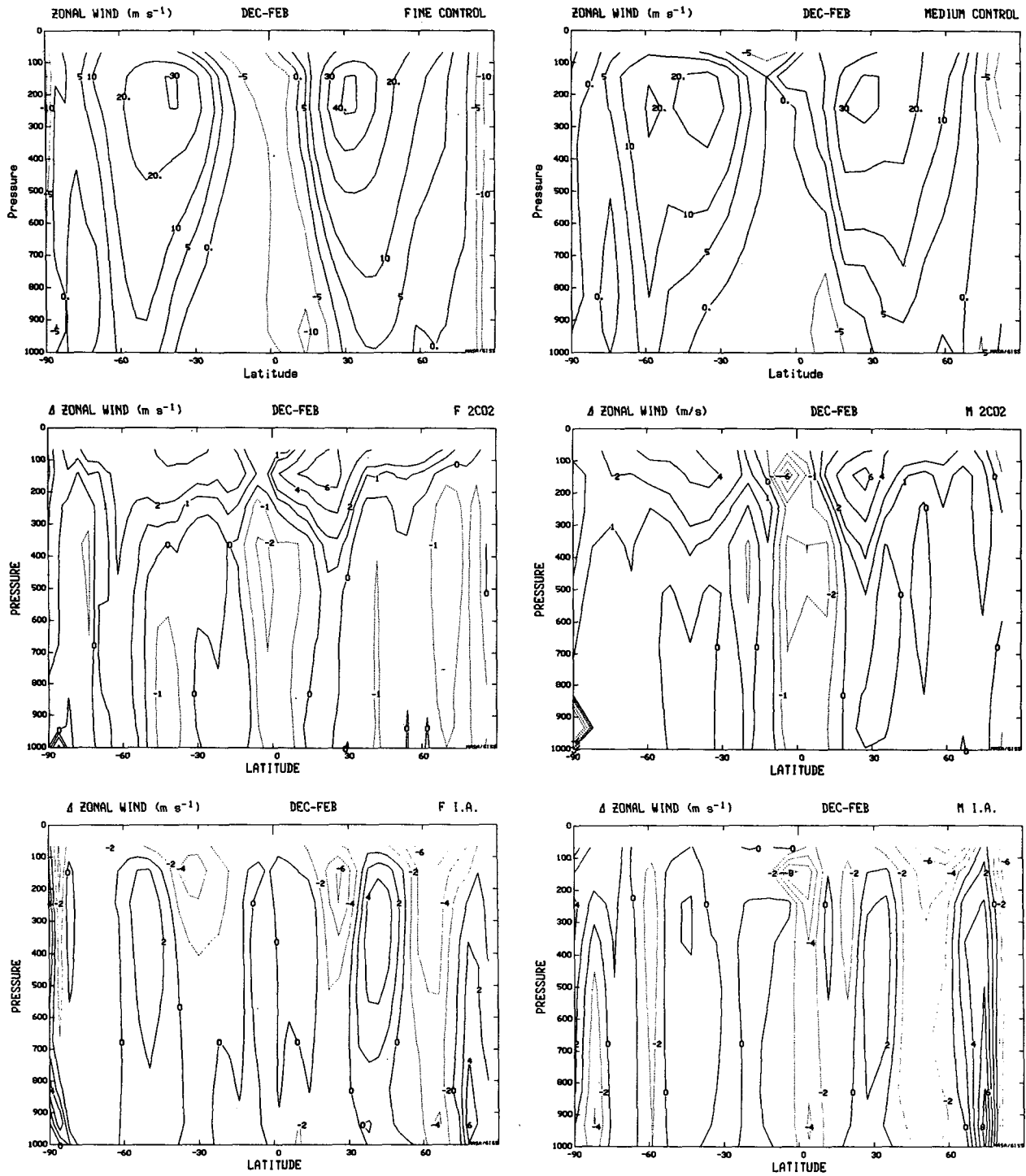


FIG. 8. As in Fig. 5 but for December–February zonal wind.

humidity, and the medium grid, with its smaller high latitude eddy energy increase, has a somewhat greater reduction. The doubled CO₂ experiments (Fig. 10, bottom left) show increased eddy latent heat transport, due to the greater moisture in the warmer atmosphere,

but the effect is less in the finer grid at midlatitudes in association with its larger eddy energy decrease.

The eddy transport of static energy combines the effects of latent and sensible heat transport. For the ice age runs, eddy energy transport increases with both

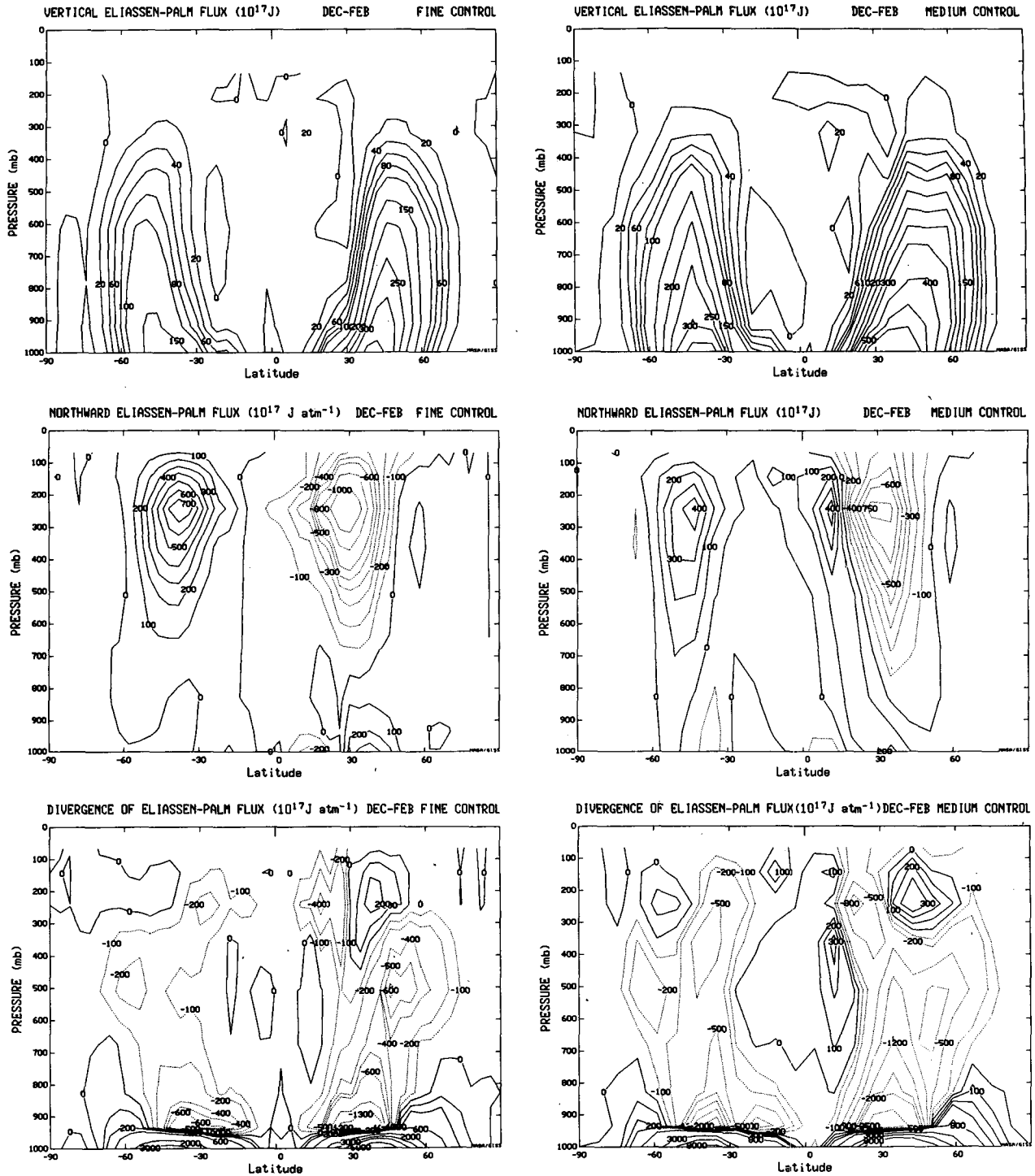


FIG. 9. Finer-grid (left) and medium-grid (right) control run values of the vertical Eliassen-Palm flux (top), northward Eliassen-Palm flux (middle), and Eliassen-Palm flux divergence (bottom).

resolutions (Fig. 11, top right), but at high latitudes it is larger in the finer grid, dominated by the sensible heat transport change. In the doubled CO_2 runs (Fig. 11, top, left), the medium and finer grid have com-

pletely different responses in the Northern Hemisphere: the medium grid shows increased eddy energy poleward transport, dominated by the greater latent heat transports, while the finer grid shows decreased eddy energy

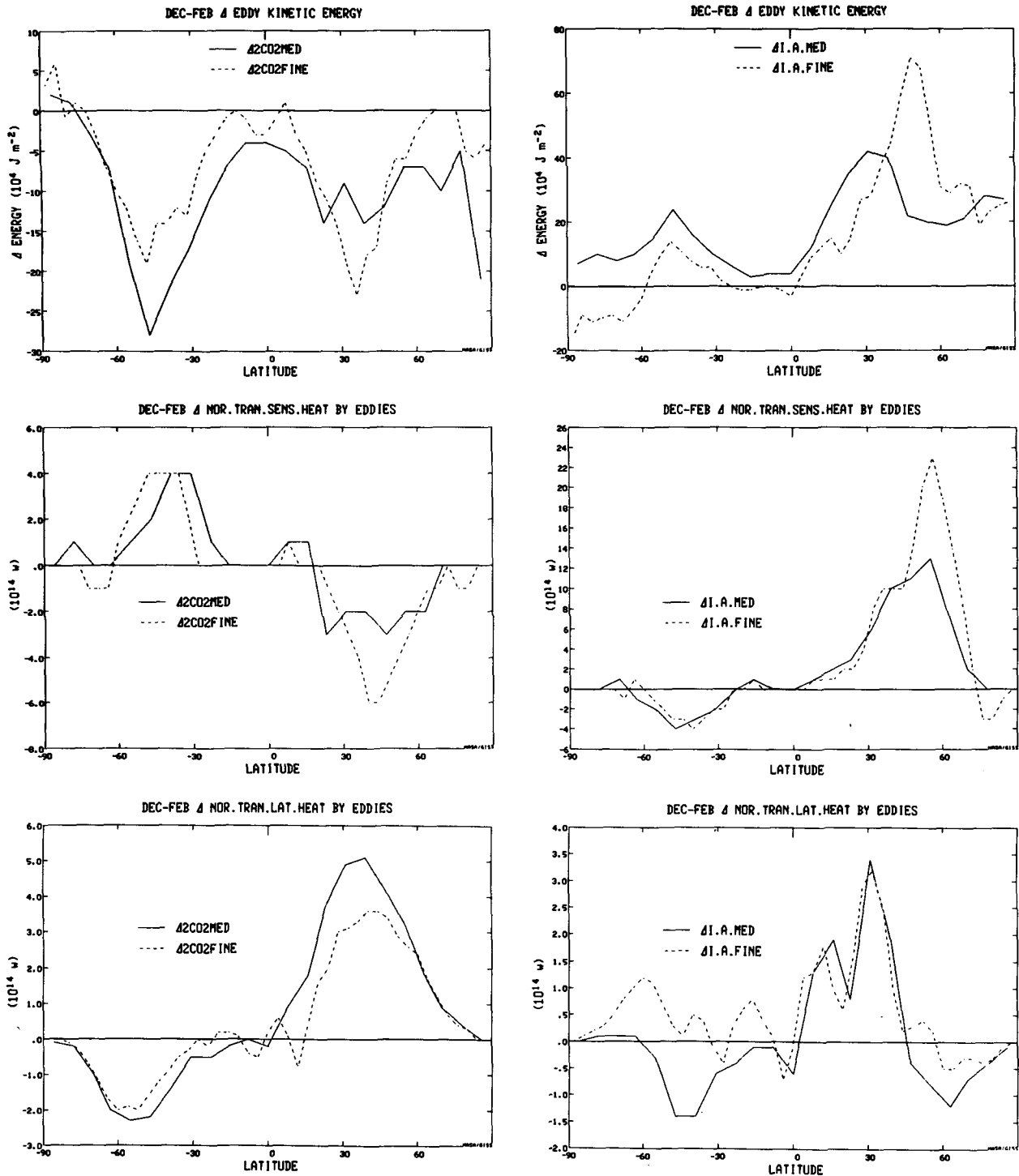


FIG. 10. As in Fig. 3 but for the December–February changes in eddy kinetic energy (top), northward transport of sensible heat by eddies (middle), and northward transport of latent heat by eddies (bottom).

transport, due to the larger reduction in sensible heat transport and smaller increase in latent heat transport. Since both resolutions are responding to the same latitudinal temperature gradient change, it is obvious there

is not a unique reaction of eddy transports to changes in the latitudinal temperature gradient.

The differences in the Ferrel cell reaction in the different experiments and resolutions (Fig. 5), resulting

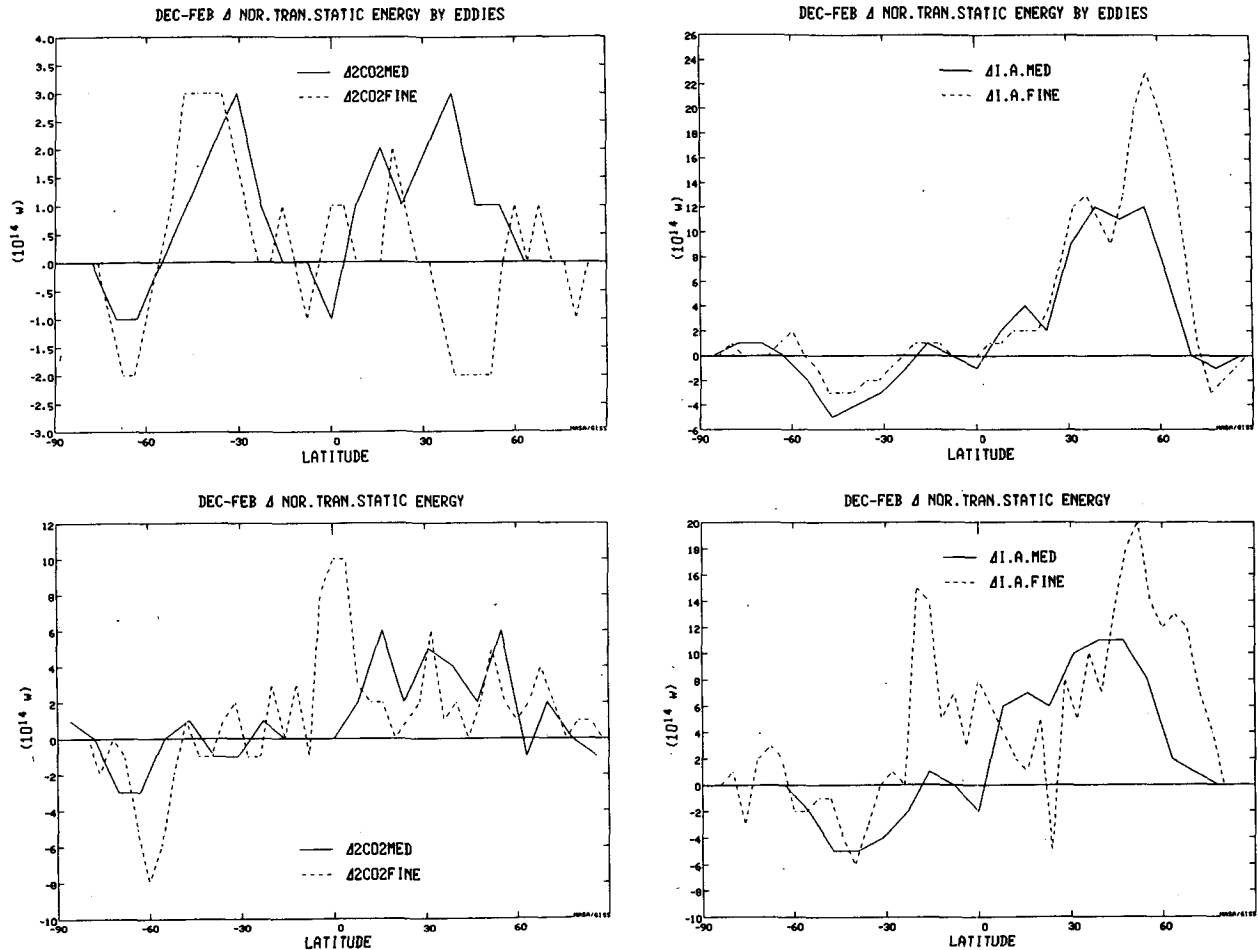


FIG. 11. As in Fig. 3 but for the December–February changes in northward transport of static energy by eddies (top) and total atmospheric northward transport of static energy (bottom).

from differences in eddy transport convergences (Table 4), can now be clarified. The greater finer grid ice age increase in Ferrel cell intensity around 60°N results from the greater energy convergence with this resolution; furthermore, the different latitudinal distributions of direct and indirect cell changes from 25°–50°N with the two resolutions result from the differing convergence and divergence of the eddy transports seen in Fig. 11 (top). Similarly, in the doubled CO₂ experiments, there is a strong eddy energy convergence around 30°N in the finer grid, which helps generate a direct cell (with negative stream function change) in midlatitudes (Fig. 5). In the medium grid, eddy energy transport divergence occurs at the same latitudes, and a slightly more low-level direct cell results.

The total atmospheric northward transport of energy includes mean circulation effects. The medium and finer grid control runs have very similar atmospheric transports with the finer grid having slightly smaller values at midlatitudes due to its greater Ferrel cell equatorward transport of geopotential energy. The

changes in the different experiments are shown in Fig. 11 (bottom). The reduction in the subtropical direct cell in the finer grid ice age experiment (Fig. 5) lowers its transport change below that for the medium grid in lower midlatitudes, although both show increased transport compared to their control runs. The increased eddy heat transport at high latitudes still allows the finer grid change to exceed that of the medium grid at upper midlatitudes and further poleward. In the doubled CO₂ experiments, the eddy transport differences at midlatitudes are still seen, but they are modified by the mean cell changes so as to show less systematic difference. In fact, the overall pattern of Northern Hemisphere atmospheric energy transport convergences and divergences look relatively similar in both resolutions.

To examine the resolution dependency of total energy transports, including that implicit in the ocean, we turn to the annual average results. The control run values of total atmospheric energy transport are still very similar, while reduced Northern Hemisphere

(N.H.) midlatitude transport (relative to the medium grid) again appears in the finer grid ice age run (Fig. 12, top right); however, both resolutions show increased poleward atmospheric transport in midlatitudes of both

hemispheres. Doubled CO₂ transports (Fig. 12, top left) differ mainly at low latitudes, where the more intense finer grid Hadley cell changes influence the results, and at upper midlatitudes, again the effect of mean circu-

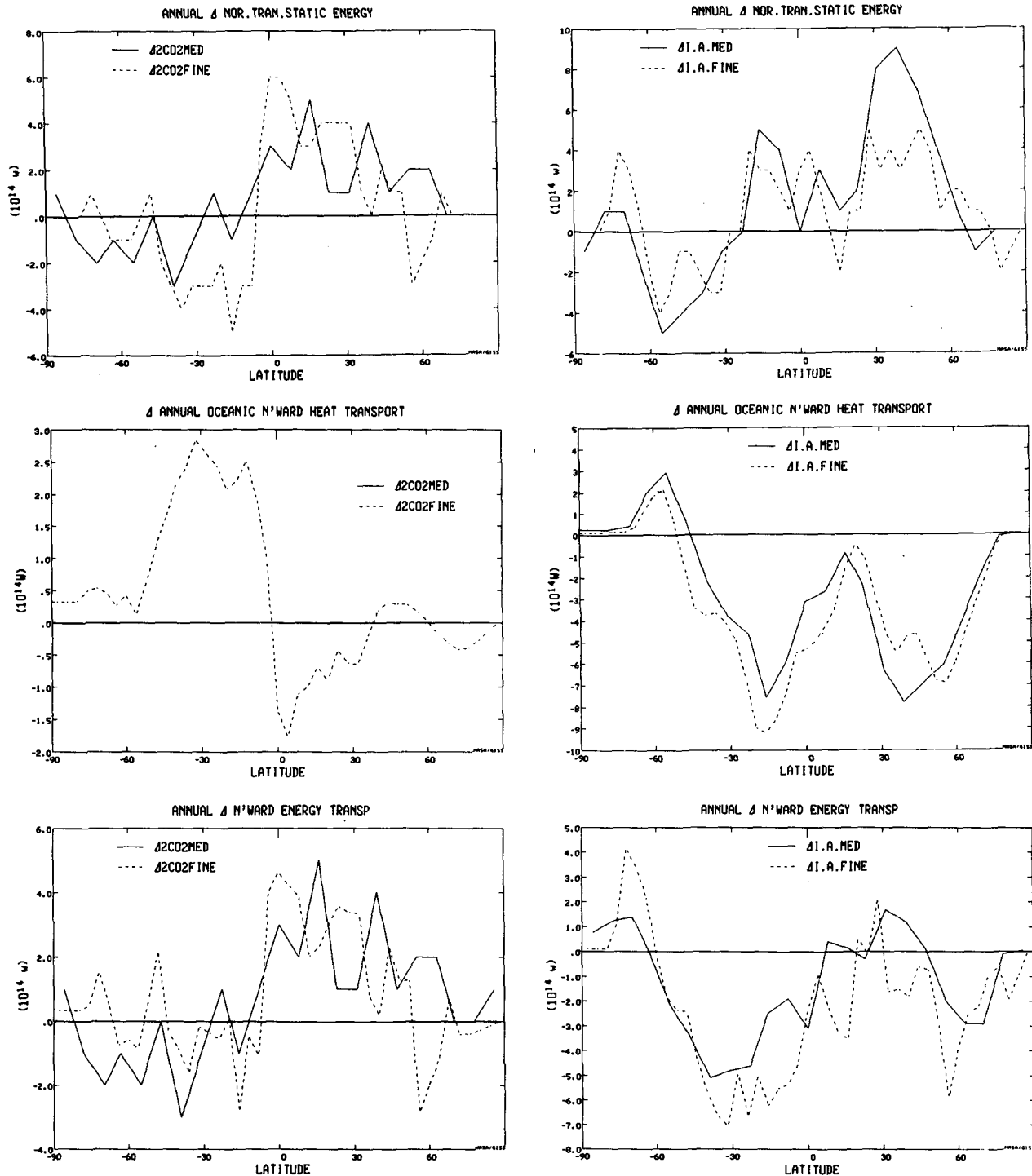


FIG. 12. As in Fig. 3 but for the annual average change in atmospheric northward transport of static energy (top), change in implied northward transport of heat in the ocean (middle), and change in atmospheric plus oceanic northward energy transport (bottom).

lation differences. In both doubled CO₂ experiments there is increased poleward transport, at least up through midlatitudes. Thus, in both the warm and cold climates, increased atmospheric energy transport occurs with the two different resolutions.

The implicit ocean transports can be obtained for the runs with specified ocean temperatures by calculating the transport convergence necessary to offset the net surface heating (Miller et al. 1983). The finer grid control run poleward ocean transports are slightly greater than medium grid values, as the greater finer-grid surface winds lead to greater heat flux losses at mid- and high latitudes. The medium-grid doubled CO₂ experiment and control have no change in heat transport, explicitly, while the finer-grid doubled CO₂ run has greater implied equatorial energy convergence (Fig. 12, middle left), to balance the large equatorial heat flux loss (Fig. 4). With finer resolution there is an overall decrease in poleward ocean heat transport, because of the slightly increased net heating at the surface from the smaller albedo and increased absorbed solar radiation (Fig. 3). The ice age ocean transport changes are similar in pattern in both resolutions, but have somewhat different values and convergences, to offset the differences in net heating (Fig. 4). Note that both show decreased poleward ocean transports at Northern Hemisphere midlatitudes, as sea ice insulates the ocean further north, with increased convergences in the subtropics to provide the warm sea surface temperatures in the CLIMAP reconstruction. (The midlatitude results differ from those of Rind (1986), where estimates were made for the winter season and its heat storage; the results are very sensitive to the heat storage assumption, and precise values cannot be calculated given the lack of knowledge about ice age mixed layer depths.)

The total energy transports and their changes can now be calculated as the sum of the atmospheric and oceanic transport effects. The control run values are very similar, with slightly greater values in the finer grid due to its slightly larger poleward ocean transports. The doubled CO₂ runs have increased poleward energy transports, except at upper midlatitudes in the finer-grid run (Fig. 12, bottom left). The ice age runs show a general tendency to decreased transports, in the Northern Hemisphere (Fig. 12, bottom right), especially in the finer grid, but increased poleward transports in the Southern Hemisphere. Obviously, no consistent relationship between the energy transport changes and the change in latitudinal temperature gradient can be found in the different hemispheres, cold or warm climates, or even, to some extent, with different resolutions.

c. Regional results

Changes in regional climate depiction as a function of resolution combine the dynamical, latitudinal distinctions discussed above, with the more local individ-

ualistic characteristics of the control runs and their responses. In addition, the finer-grid runs can obviously produce results with greater resolution, depicting local concentration gradients unavailable on the medium grid. All three effects appear in the results presented below.

The sea level pressures generated by the medium- and finer-grid control runs and the changes in the experiments are shown in Fig. 13. The finer grid produces a more realistic Northern Hemisphere sea level pressure field, with broader and deeper subpolar lows, (Fig. 13, top), a direct result of the greater long wave/medium wave energy distribution.

In the ice age runs, the increase in sea level pressure above the ice sheets is similar with both resolutions, but the regions of relative pressure decrease over the Northern Hemisphere oceans are shifted southward in the medium grid (Fig. 13, middle). (Note that the increase in global mean sea level pressure of 12.5 mb, due to the altered ice sheet topography, has not been subtracted out). With increased eddy kinetic energy in the ice age simulations, low pressure systems intensify; as the location of the low pressure systems is somewhat different in the different resolution control runs, their intensification will appear as relative sea level pressure decreases in different locations. In addition, the pattern of change shows a smoother, longer-wave appearance in the finer grid, as its long-wave energy increased more with that resolution, while the medium grid showed greater energy changes, relative to the finer grid, in intermediate scale wave energy (Table 6, Fig. 7). The results for the two doubled CO₂ experiments show the same processes at work, although now the eddy kinetic energy decreases, so the synoptic-scale systems weaken. It is apparent that changes at any individual location can be very different in the different resolution experiments.

The same distinctions apply throughout the troposphere. The changes in the 500 mb height fields for December–February are shown in Fig. 14, with broader-scale patterns of change and some shift in position in the finer grid for both the warm and cold climates. Note in particular the relative trough which develops in the ice age climate over Greenland in the finer grid, while its medium grid counterpart, like the surface effect, is further south and west.

Associated with these alterations in the geopotential surfaces are changes in jet stream (Fig. 15) and other tropospheric wind patterns. Tropospheric advection changes will thus also be resolution dependent. Differences with resolution in the doubled CO₂ subtropical jet stream response over North America affect the depiction of storm track and winter precipitation changes (Rind 1988). Jet stream splitting over the ice sheets, apparent as a change to more westward flow over southern Canada and northeastern North America, has a somewhat different appearance in the two resolutions, indicating, among other things, the influence of the

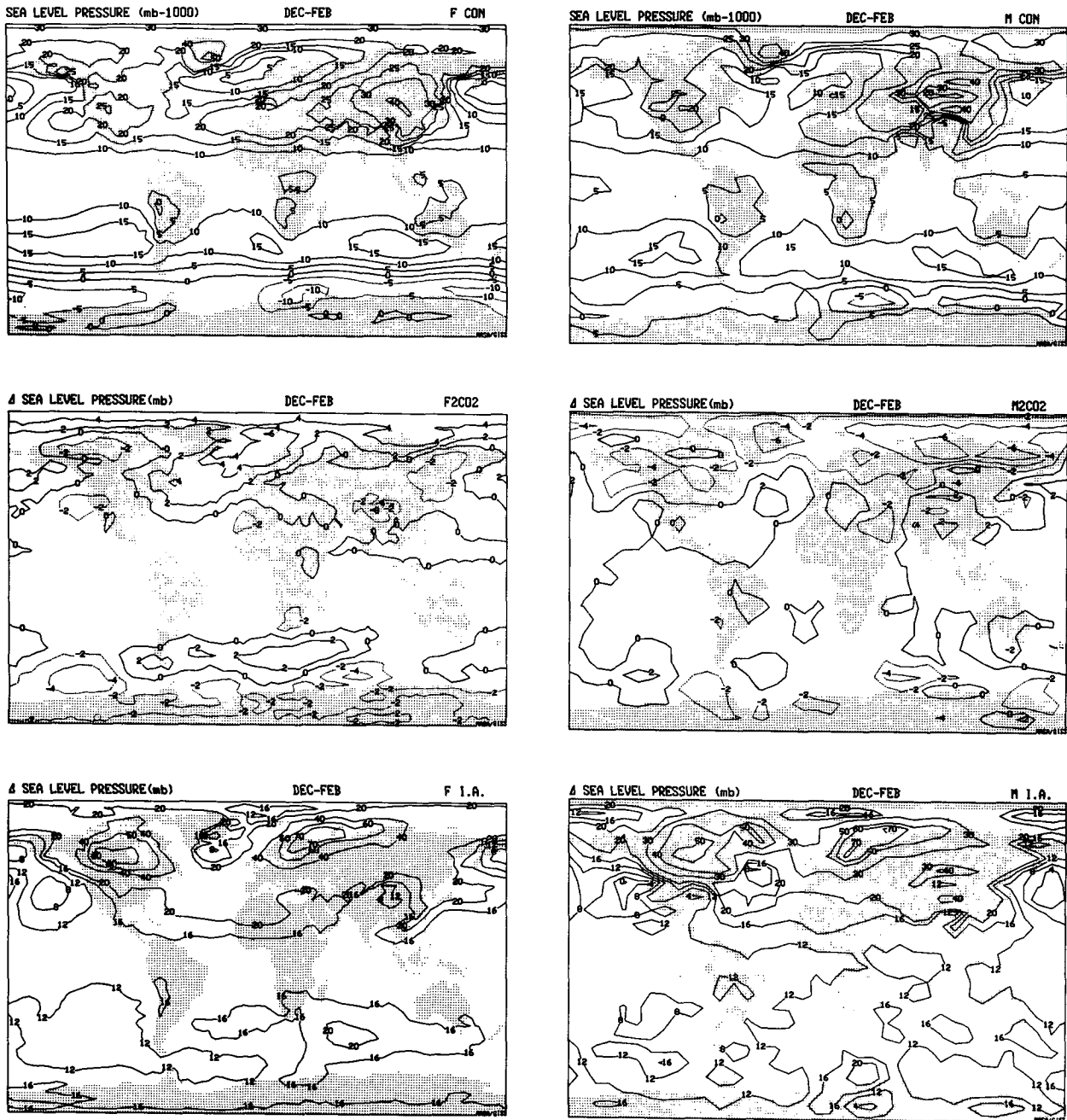


FIG. 13. Finer-grid (left) and medium-grid (right) December–February sea level pressure in the control runs (top) and change in sea level pressure in the doubled-CO₂ (middle) or ice age (bottom) climates. Note the excess ice age sea level pressure of 12 mb has not been subtracted.

differing resolution of topography. Neither result is very similar to the topographic avoidance shown by Kutzbach and Wright (1985).

The surface wind and temperature changes from December–February are shown together for the doubled CO₂ experiments in Fig. 16. Differences in the sea level pressure changes lead to differences in surface wind velocity changes, with resulting differences in

thermal advection and local temperature change patterns. For example, stronger warming occurs west of Greenland in the finer-grid run in association with a change to more northward flow, while the medium grid has more southward flow in the same area (Fig. 16). The medium grid warming in the Middle East is greater, in conjunction with increased winds from the south. In the ice age experiments for this season, the

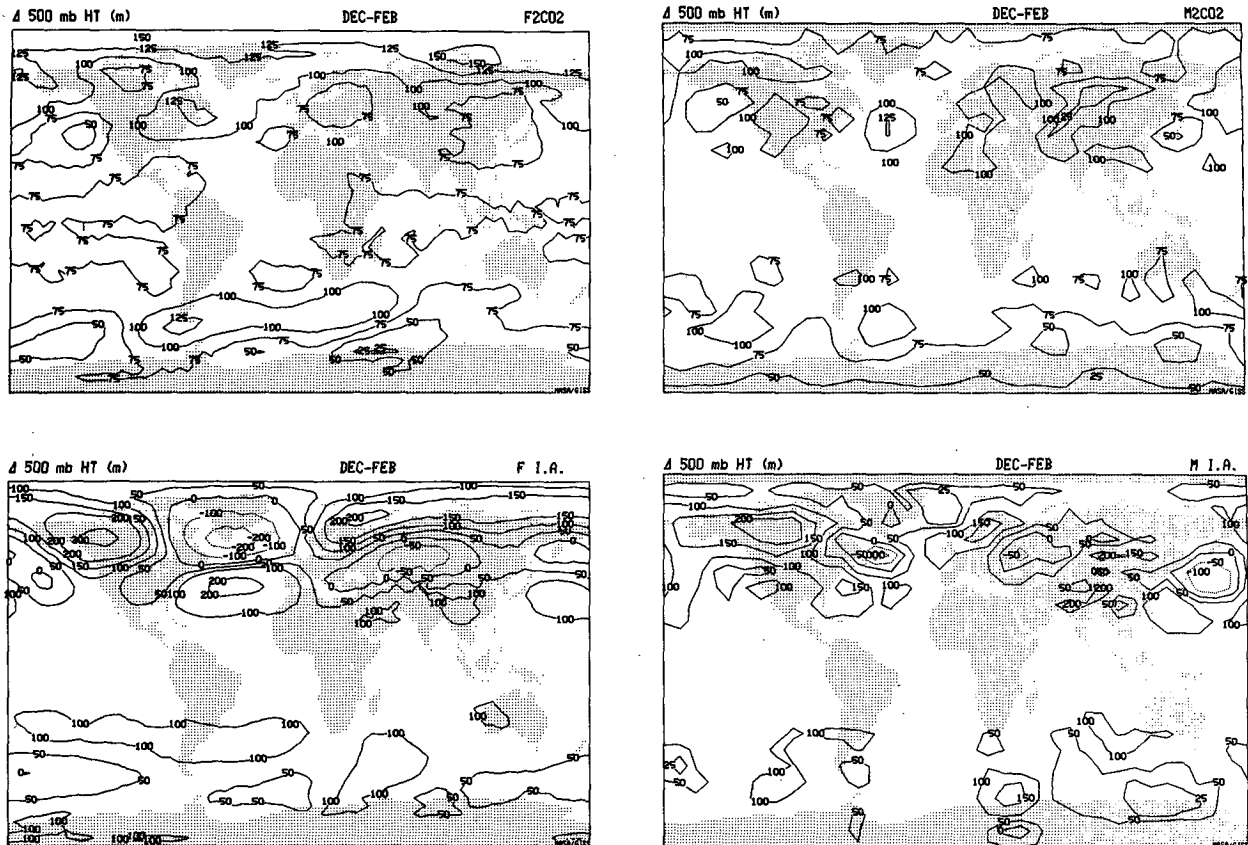


FIG. 14. Finer-grid (left) and medium-grid (right) December-February change in 500 mb height in the doubled- CO_2 (top) and ice age (bottom) climates.

fine grid produces warming in Alaska and southeast Asia, again associated with increased south winds, an effect which is mitigated or nonexistent in the medium grid whose wind flow change is different. As the sea surface temperature changes are identical, the different resolutions produce equivalent effects over the ocean, and in the ice age experiments the ice sheets produce similar cooling in their vicinity.

In June-August (Fig. 17), the ice age maximum summertime warming over the Asian continent, a result of subsidence over the ice sheets and increased low-level southerly flow, occurs further south in the medium-grid run, in accordance with its wind field changes at both lower and upper levels (Fig. 17, top, middle). This feature appears with different magnitudes and at different locations in the various ice age models (Rind 1987a), mirroring the variability noted here. The results in Fig. 17 emphasize the caution which needs to be applied when comparing regional climate model output to local paleoclimate indicators.

The annual average precipitation in the control runs is shown in Fig. 18 (top). The finer grid produces drier deserts (more realistic), but much wetter tropical rain belts (less realistic). In general, finer grid rainfall is ex-

cessive in the rainy belts, whether it be the intertropical convergence zone, or the storm tracks in winter. This is associated with the greater instability and penetrative convection possible on the smaller grid, and the increased evaporation associated with the stronger surface winds with the finer resolution. The increased rainfall produces more intense local meridional cells, whose subsidence helps dry out desert regions; as noted above, the finer-grid Northern Hemisphere winter Hadley cell appears to have too sharp an equatorial cutoff associated with the heavy rainfall. This illustrates that a finer-resolution model is not necessarily more realistic in all respects.

The annual average precipitation changes for the different experiments (Fig. 18, middle, bottom) show that many similarities exist for the different resolution results in both the warm and cold climate changes, due to the strength of the (similar) surface forcing. However, the finer-grid results show a broader pattern of change, zonally oriented, than does the medium grid. This is consistent with the more intense low-latitude mean circulation changes in the finer resolution, implying more zonal consistency, and the predominance of the finer-grid lower wavenumber changes (Table 6b).

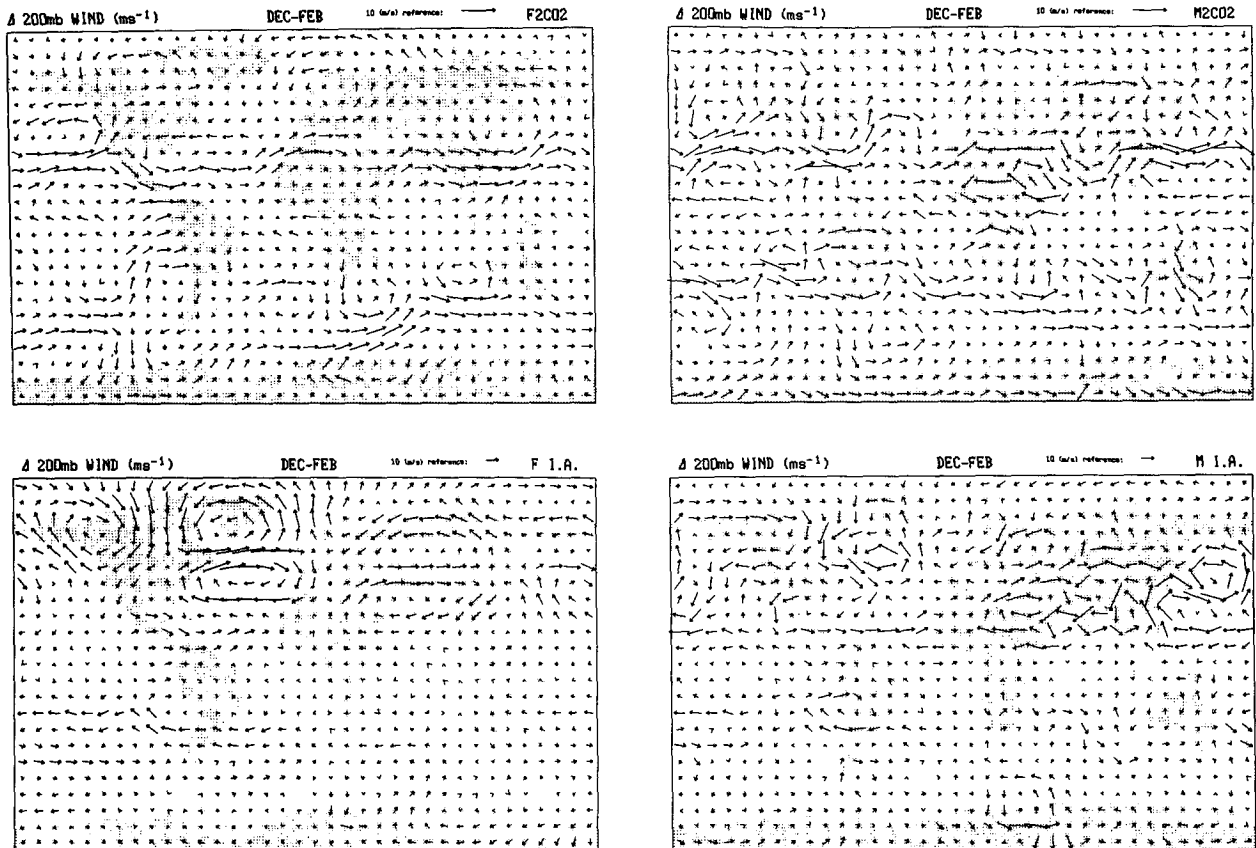


FIG. 15. As in Fig. 14 but for the change in 200 mb wind in Dec-Feb. To facilitate comparison, the finer-grid winds have been averaged onto the medium grid in this and subsequent wind presentations.

4. Summary and discussion

a. Climate model resolution effects

The results detail the ways in which the atmospheric dynamics and regional depictions of warm and cold climate changes depend upon characteristics of the control runs influenced by their resolution. The differences between the finer- and medium-grid present climate simulations revolve around two processes: nonlinear energy transfer, and moist convection. The finer grid has increased nonlinear energy transfers to long waves and to the zonal mean flow. Zonal winds are thus stronger throughout the atmosphere, producing increased evaporation and surface heat flux losses. The increased evaporation leads to a general increase in the hydrologic cycle, with more precipitation, latent heat release and a warmer atmosphere. The greater moisture availability combines with a moist convective scheme that is more penetrative on the finer grid (as greater degrees of instability are possible on the smaller grid), to produce effects such as increased penetrative convection and increased warming of the upper troposphere, decreased high-altitude tropical cloud cover

and planetary albedo, and increased net radiation at the surface. The increased tropical precipitation provides for a sharper low-latitude cutoff of the Hadley circulation.

At the same time, the stabilizing effect of the increased penetrative convection leads to a decrease in shallow and midlevel convective mass flux. With reduced moist convective mixing of momentum, east winds at low and subtropical latitudes are stronger, which prevents upward penetration of eddy energy. The increased nonlinear energy transfer strengthens standing long waves, but reduces eddy energy overall, so there is also decreased upward energy flow from mid-latitudes. There is then less EP flux convergence in the subtropical jet stream region, and stronger jet streams. This is part of the overall barotropic transfer of eddy to zonal kinetic energy, equivalent to the nonlinear energy transfer into wavenumber zero which produces the stronger surface winds and hydrologic cycle. As eddy energy transports are not overly affected, the increased resolution allows for stronger eddy transport convergences and a stronger Ferrel cell. The decrease of medium-scale energy results in a change in the sea level pressure distribution patterns, while the increased

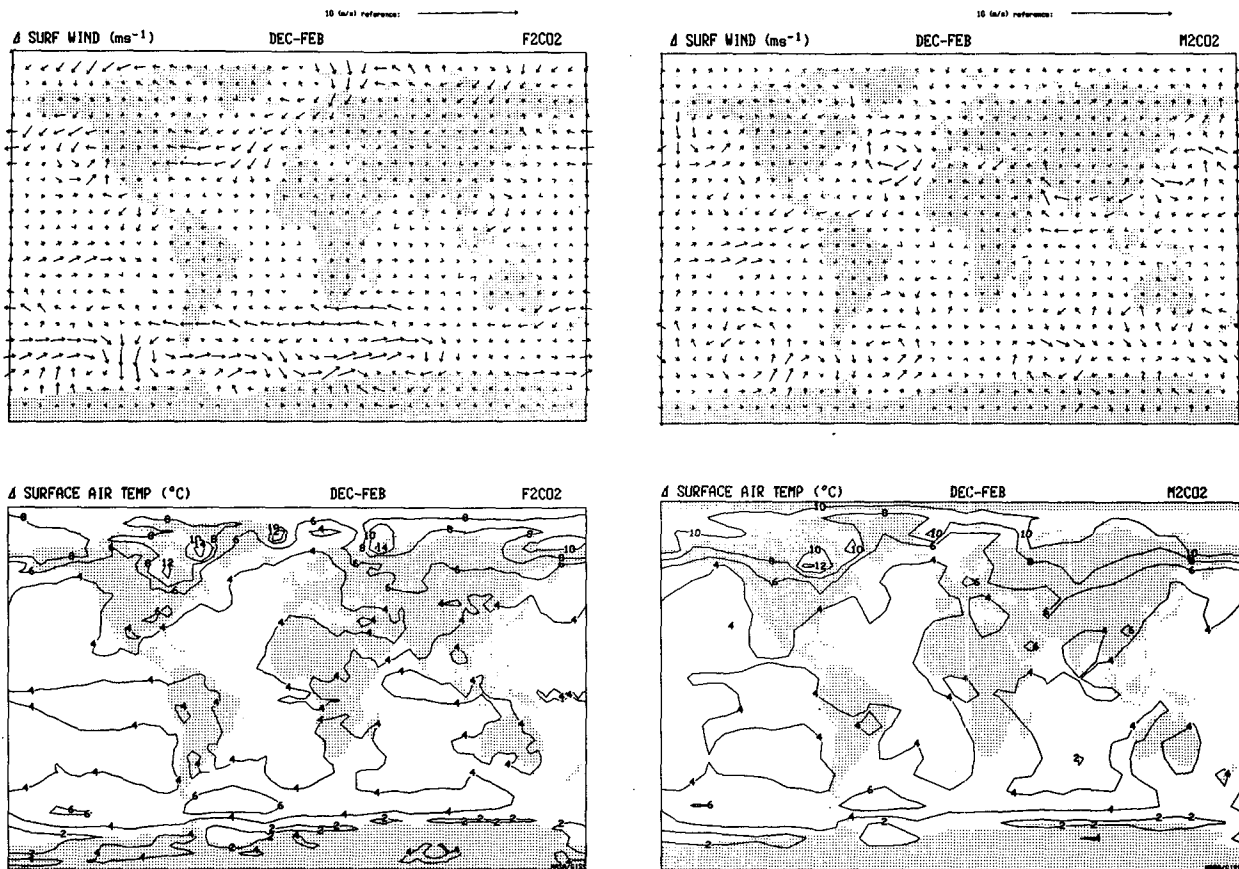


FIG. 16. Finer-grid (left) and medium-grid (right) change in surface wind (top) and surface air temperature (bottom) for the doubled- CO_2 climate in December–February.

moist convective rainfall produces wetter tropical and drier subtropical regions.

The climate change experiments show the impact of these differences. Table 7 summarizes some specific differences in the control runs, and the changes with resolution in the climate experiments. The finer-grid doubled CO_2 experiment shows a greater increase in evaporation, precipitation, penetrative convection, and net radiation at the surface, while the ice age finer-grid experiment shows greater decreases in these quantities. All are processes which are of greater magnitude in the finer-grid control run than in the medium grid. The finer-grid ice age experiment shows a greater increase in long wave/intermediate wave energy ratio, poleward eddy energy transports, and Ferrel cell intensity, while the finer grid doubled CO_2 experiment shows greater decreases in these values. The finer-grid control run Ferrel cell was stronger, as was its standing long wave energy, although the eddy energy transports were similar. Other processes, such as the change in low-latitude east winds, depended on specific conditions in the control run; e.g., only the medium-grid doubled CO_2 run has stronger tropical easterlies, as the reduced vertical flux of eddy energy is confined to midlatitudes in the

finer grid (due to the subtropical east winds in the control), so reduced tropical EP flux divergences occur only in the medium grid warm climate.

There is thus an overall tendency for the climate change experiments to amplify processes which occur with greater frequency in their respective control runs. For both the nonlinear energy transfers in the momentum equation and moist convection, the finer-resolution model acts differently simply because it is capable of producing convergences over smaller grids, resulting in larger magnitudes. With finer resolution, the finite difference equation better approximates the differential equation, and produces faster moving transient eddies; in the finer-resolution control run, the transient eddies transport more momentum relative to the standing eddies (Table 5), with the larger eddy momentum transport an expression of the increased magnitude of the nonlinear term. While this allows the finer resolution model to produce more realistic simulations for some features (e.g., a better Ferrel cell resulting from larger eddy transport convergences), improvement is not guaranteed. As noted earlier, while the eddy momentum transport poleward of the jet stream appears more reasonable in the finer-grid con-

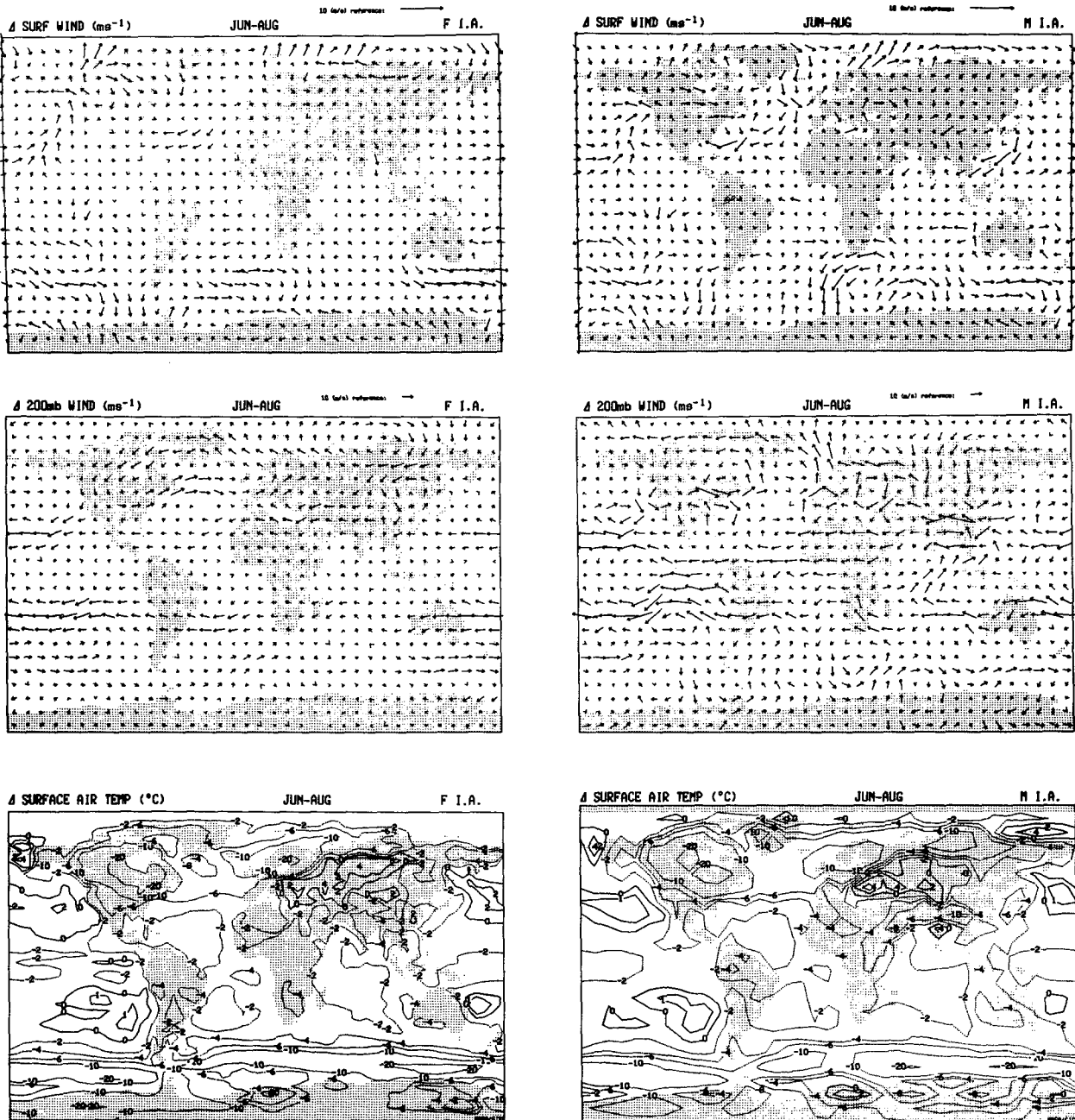


FIG. 17. Finer-grid (left) and medium-grid (right) change in June–August surface wind (top), 200 mb wind (middle), and surface air temperature (bottom) for the ice age climate.

trol run, it is less realistic in the region north of the equator.

To evaluate the realism of the energetics on the different resolutions, we compare the energy budgets for the different wavenumbers with observations (Table 6a). The energy transfer processes producing zonal kinetic energy are more realistic with the finer resolution; however, the nonlinear transfer of energy out of the

long waves and into the zonal mean flow appears to be exaggerated in the finer grid, while it is perhaps underestimated on the medium grid. Clearly the magnitude of the intermediate-scale energy looks more realistic in the medium-grid run, while long wave energy is underestimated with both resolutions; thus, the improved appearance of the monthly mean sea level pressure field with finer resolution may be misleading.

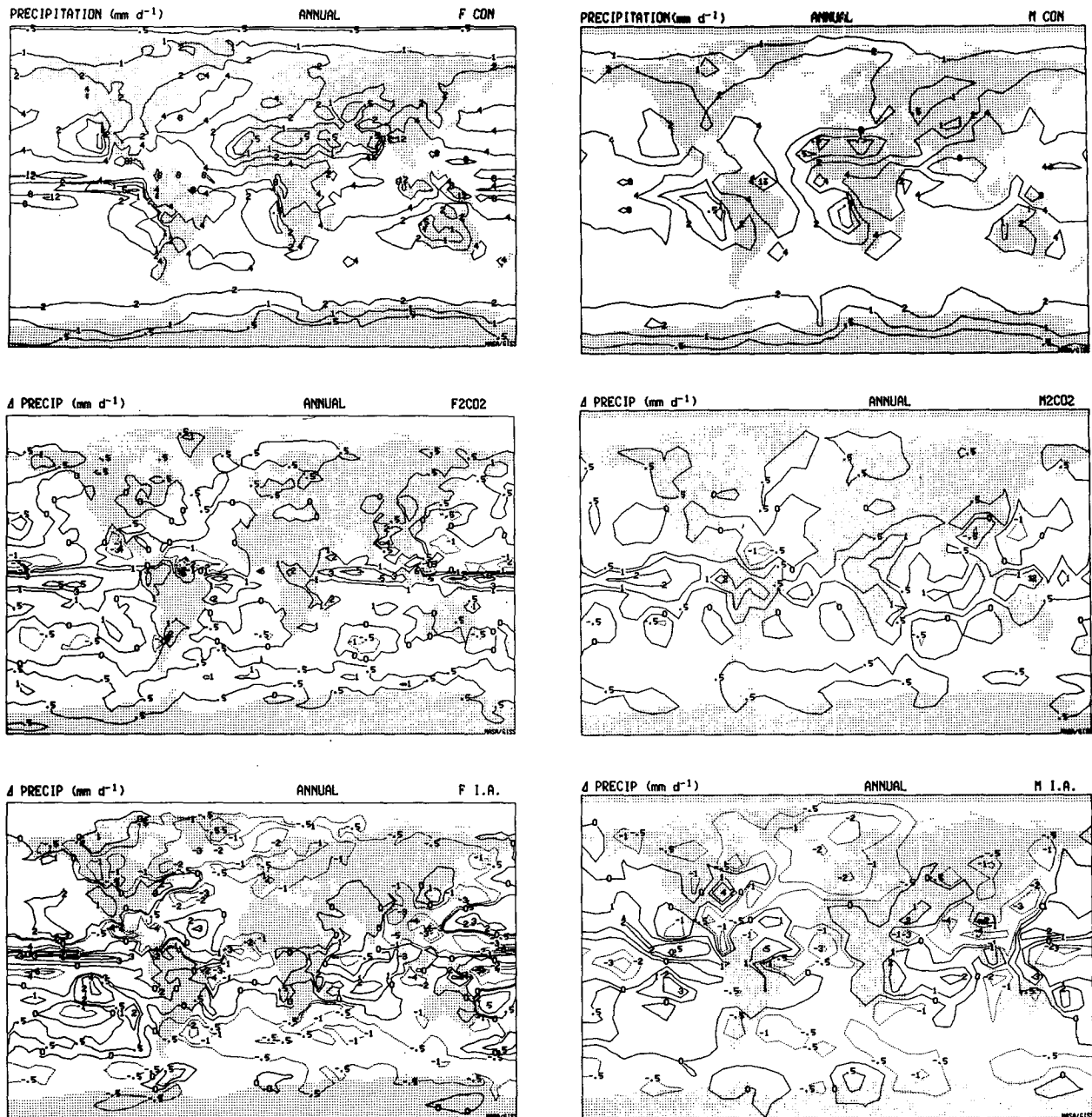


FIG. 18. Finer-grid (left) and medium-grid (right) annual average precipitation for the control runs (top), and for the changes in the doubled- CO_2 (middle) and ice age (bottom) climates.

(However, note that uncertainty exists in the accuracy of the observed values averaged over the entire hemisphere; for example, comparison of the modeled and observed zonal wind fields implies it is somewhat doubtful that the finer-grid model is really underestimating the zonal kinetic energy, as indicated in Table 6a.) The larger-magnitude convective precipitation is unrealistic in some locations in the finer grid where the medium grid produces better values (Fig. 18), al-

though the deserts are generally drier and better simulated with the finer resolution; nevertheless, the climate feedback may depend more on the former than the latter. Overall, then, the finer resolution produces mixed benefits in the present climate simulation, and if the criteria for correct prediction of climate change is a more accurate control run, it is not clear which model is to be preferred.

It is important to understand whether nonlinear en-

TABLE 7. Summary of control and climate change resolution differences.

Finer-grid control compared to medium	Climate change compared to med
1. Greater longwave/intermed. wave k.e. ratio	1. Greater increase (I.A.) or decrease (2CO ₂) in ratio
2. Less eddy kinetic energy	2. Greater increase (I.A.) or decrease (2CO ₂) at mid lat
3. Stronger Ferrel Cell	3. Greater increase (I.A.) or decrease (2CO ₂)
4. Similar poleward eddy transports	4. Greater increase (I.A.) or decrease (2CO ₂)
5. Greater zonal kinetic energy	5. Greater increase (I.A.) or smaller increase (2CO ₂)
6. Greater surface fluxes	6. Greater increase (2CO ₂) or decrease (I.A.)
7. Greater precipitation	7. Greater increase (2CO ₂) or decrease (I.A.)
8. Greater penetrative convection	8. Greater increase (2CO ₂) or decrease (I.A.)
9. Warmer atmosphere	9. Greater increase (2CO ₂) or decrease (I.A.)
10. Better regional albedo discrimination	10. Greater increase (I.A.) or decrease (2CO ₂)

ergy transfers really are excessive with the $4^\circ \times 5^\circ$ resolution, whether this error is amplified as the spatial scale decreases further, and how it relates to other model processes. While some of the tendencies reported here are likely to be model dependent, it is interesting that both grid-point and spectral models produce increased zonal kinetic energy as resolution is increased. Recent results obtained using the ECMWF model (Arpe and Klinker 1986), the UKMO model (Mitchell et al. 1987) and the NASA Goddard Laboratory for Atmospheres (GLA) model (Tenenbaum 1987), all with 200–300 km resolution, have duplicated the earlier studies in finding excessive tropospheric zonal wind velocities. Tenenbaum (1987) has shown that parameterized orographic drag solves only part of the problem and suggests other drag mechanisms be incorporated, such as convective and shear-generated gravity waves used by Rind et al. (1988) in their climate/middle atmosphere model. If the nonlinear transfer of energy into the zonal flow is being done correctly, then the excessive zonal flow may well be resulting from incorrect dissipation mechanisms, and there is good reason to believe that current models are incapable of properly generating gravity waves and gravity wave breaking (Rind et al. 1988). If the nonlinear term is overestimated, it could still be related to inadequate dissipation, which allows wind magnitudes to build sufficiently to force excessive nonlinear transfers. In grid point schemes, the problem may also be associated with inaccurate numerical solution of the momentum equation; Russell (personal communication) has been

comparing numerical schemes, and has found that the nonlinear transfer of energy to the zonal mean flow does differ with different schemes, especially on coarser resolutions. For example, enstrophy-conserving solutions would be expected to have better energy transfer characteristics than schemes without that property. If the numerical scheme is at fault, then additional drag mechanisms will act as palliatives to relieve the symptom, a practice which to some extent has been legitimized by the use of numerical diffusion. The zonal kinetic energy budget in high-resolution models needs to be closely investigated.

Convective parameterizations will also generally be sensitive to resolution. In any scheme with an “on/off” switch for convection, such as the exceeding of some instability criterion, it will always be easier for the necessary convergences and instability to be achieved with finer resolution. In addition, extreme instability values will also be easier to obtain, and the finer-resolution model will then produce more heating at higher altitudes due to its greater penetrative ability. Differences in penetrative convection brought about by different convection schemes is one possible reason for the different low-latitude responses of the GISS and GFDL doubled-CO₂ models (e.g., Rind 1987b). Furthermore, if the convective scheme relates the convective mass flux moved to the size of the grid box, this too will differ with resolution; in conjunction with the instability criteria, it will produce results such as those shown in this study of resolution-dependent, low-latitude temperature and wind profiles. A more reasonable approach would be to include a continuous spectrum of convective scales and mass fluxes, as employed in the GISS model 1 (Hansen et al. 1983). As increasingly finer-resolution models are developed and employed, these issues will have to be addressed, if climate change depictions are to maintain any consistency.

b. Atmospheric dynamics

In the rest of this section, we relate the climate change results obtained with the different resolutions to topics previously studied with a particular resolution. Rind (1987b) generalized results from previous studies about the dynamical reactions to climate change of features such as the Hadley cell, subtropical jet stream, ratio of stationary to transient eddy energy, the energy cycle, and the feedback of total energy transports to climate change. We treat each of these features separately.

1) HADLEY CELL

Rind and Rossow (1984) discussed a range of physical processes potentially capable of affecting the Hadley cell. The differing response of the doubled-CO₂ Hadley cell with the different resolutions (Fig. 5) emphasizes that the calculated Hadley cell changes will also be affected by the convective scheme and grid resolution.

The increased and more sharply delineated convective rainfall characteristic of the finer grid allowed the doubled-CO₂ finer-grid experiment to produce a more intensified low-latitude Hadley cell, as well as a more well-defined decrease in the subtropical portion of this cell. The resolution dependency of the change in latitudinal extent of the Hadley cell (Table 5) in the ice age climate is related to the resolution-dependent change in eddy energy characteristics and eddy energy convergences (i.e., change in Ferrel cell strength and location). Neither the change in peak Hadley cell intensity or latitudinal extent is particularly large (Table 5), although the differences with resolution could have significant effects on the hydrological cycle in certain locations.

2) SUBTROPICAL JET STREAM

Previous studies with the GISS model (Rind 1986, 1987a,b) have concluded that the momentum balance at the jet stream level results from a sensitive balance between mean circulation effects, eddy forcing, and dissipation. Given the resolution-dependent changes in all three of these processes, it is no surprise that the jet stream response with climate change also varies with resolution. This is seen most strikingly in the ice age experiments, where the jet stream increases in the medium resolution runs, but decreases with the finer grid. In mechanistic terms, the Coriolis effect on the increased meridional wind overcomes changes in eddy deceleration in the medium grid, but not in the finer grid, processes which relate to the convective and eddy energy propagation differences described above.

3) STATIONARY-TO-TRANSIENT-EDDY ENERGY

The previous studies have examined how this ratio varies with latitudinal and longitudinal temperature contrasts, as well as topography. The only experiment in this study to show a substantial change in this ratio is the finer-grid ice age run, in which stationary eddy energy increases significantly. The result is apparently associated with the increased ice age topographic resolution available on the finer grid; as noted in Rind (1987a), an accompanying thermal effect arises due to decreased greenhouse capacity in the thinner atmosphere above. The consequences of this resolution-dependent difference for the location of the standing wave patterns and their changes can be seen in the pressure and wind field changes (Figs. 13–17). Note that in the doubled-CO₂ runs there is little change in this ratio, as the land/ocean contrast and topography difference between experiment and control do not depend on resolution. It is also interesting that in the two sets of control runs, the finer-grid ratio of stationary to transient eddy energy is not consistently larger than the medium-grid value (Table 5), even though its topography is better defined; apparently other aspects, such

as the nonlinear energy transfers associated with the better movement of the transient eddies and their momentum transport affect this ratio.

4) ENERGY CYCLE

The changes in the energy budget terms and the energy cycle are qualitatively similar in both resolutions. In the doubled-CO₂ experiments, decreases in zonal and eddy available potential energy led to decreases in energy transfers from potential to kinetic energy (Table 5a), while there was increased energy transfer from eddy to zonal kinetic energy. Overall, zonal kinetic energy increased, while eddy kinetic energy decreased. In the ice age runs, increased eddy available potential energy led to increased conversion to eddy kinetic energy, but increased zonal available potential energy was associated with decreased transfer to zonal kinetic energy; there were also large increases in transfers from eddy to zonal kinetic energy, with the net result that both eddy and zonal kinetic energy increased (Table 5b). Quantitatively differences do appear with resolution, and, as noted, the proportional increase in zonal kinetic energy is twice as large in the doubled-CO₂ medium grid, while the proportional increase in eddy kinetic energy is twice as large in the ice age finer grid.

5) TOTAL ENERGY TRANSPORTS

Changes in poleward energy transport result from hydrologic and eddy processes, both of which differ with resolution, so the transports differ as well. The doubled-CO₂ experiments have a reduced latitudinal temperature gradient in both hemispheres, and the atmospheric and total poleward energy transports increase, except in the finer resolution at upper midlatitudes. In the ice age experiments, there is an increased latitudinal temperature gradient, and poleward atmospheric transports again increase, at least at midlatitudes, while total energy transports increase in the Southern Hemisphere and decrease in the Northern Hemisphere, especially in the finer grid. There is thus no consistent feedback to a change in latitudinal temperature gradient, at least partly because of hydrologic cycle effects; this is a conclusion derived previously (Rind 1986, 1987a,b), and one which is at variance with formulations used in energy balance models.

c. Regional results

Many doubled-CO₂ regional changes are resolution dependent. As discussed in detail, (Rind 1988), doubled-CO₂ variations in the hydrologic cycle over the United States show this effect due to changes in precipitation with different grid size (e.g., Fig. 18), as well as changes in runoff. The finer-grid control run has a better depiction of the western United States mountain topography, which limits the ability of the model to

advect moisture eastward from the Pacific; in the doubled-CO₂ run, this limitation also acts to keep the summer precipitation change smaller than that for the medium grid (Rind 1988). Furthermore, the finer-grid control run has better resolution in the northwestern portion of the United States, so that grid boxes can exist with a mean temperature below 0°C for several months, and maintain significant snowcover. In the medium grid control run, the bigger grid boxes extend to lower latitudes, have warmer temperatures, and less snow. The finer grid doubled CO₂ run can thus lose more snowcover, and the added reduction leads to a decrease in spring runoff and soil moisture not seen in the medium-grid run. These inherent resolution-dependent characteristics combine with the differing dynamics and convection to produce a variety of changes in hydrologic properties, wind fields, temperature and cloud cover as a function of resolution.

Results of the changes during June–August for several of these quantities averaged over specific geographic regions are given in Table 8a. The doubled-CO₂ climate changes often show large variation with resolution, within the overall context of the warming. For example, soil moisture changes in the China desert and African Sahel are of different sign and large magnitude in the two resolutions. Regional climate change impact assessments would be extremely difficult under such circumstances. Considering that the two doubled-CO₂ climate experiments have the same sea surface temperatures, global temperature change and high latitude amplification, it is little wonder that large differences exist among the results of the different modeling groups, in which these parameters differ as well.

Changes in regional quantities during the ice age are shown in Table 8b. Again, some resolution-dependent differences exist, although here the organization pro-

TABLE 8. June–August regional climate changes.

Region	Res	Δ Temp (°C)	Δ Prec (mm d ⁻¹)	Δ Evap (mm d ⁻¹)	Δ S. mois (cm)	Region	Res	Δ Temp (°C)	Δ Prec (mm d ⁻¹)	Δ Evap (mm d ⁻¹)	Δ S. mois (cm)
(a) 2CO ₂ experiments						(b) Ice age experiment					
Western U.S.	F	5.3	-0.1	0.2	5.3	Western U.S.	F	-6.0	0.8	0.3	32.9
	M	4.0	0.5	0.6	11.3		M	-5.2	0.0	-0.3	30.3
	S.D.-M	1.13	0.5	0.5	12.6		S.D.-F	0.4	0.1	0.2	7.8
Mid U.S.	F	5.4	-0.4	-0.2	-4.5	Mid U.S.	F	-11.4	-0.9	-1.3	81.4
	M	3.8	0.1	0.1	-8.1		M	-9.6	-1.1	-1.5	87.0
	S.D.-M	0.8	0.6	0.4	14.9		S.D.-F	0.9	0.6	0.4	9.2
Eastern U.S.	F	4.8	0.2	0.0	-16.9	Eastern U.S.	F	-14.1	-0.3	-1.3	N.A.
	M	3.4	0.8	0.6	-2.3		M	-10.7	2.4	-0.5	N.A.
	S.D.-M	0.9	0.8	0.5	22.8		S.D.-F	0.5	0.5	0.3	15.9
S. Canada	F	5.2	-0.3	0.2	-18.9	S. Canada	F	-20.2	-1.2	-2.2	N.A.
	M	3.0	0.4	0.6	20.0		M	-17.3	-0.2	-2.7	N.A.
	S.D.-M	0.7	0.2	0.1	25.6		S.D.-F	0.8	0.4	0.2	11.5
Greenland	F	2.9	1.0	-0.2	-0.6	Greenland	F	-8.0	-1.0	-0.2	N.A.
	M	2.3	0.3	-0.1	-5.3		M	-9.6	-1.0	-0.1	N.A.
	S.D.-M	0.5	0.2	0.1	0.2		S.D.-F	0.7	0.3	0.0	1.9
China desert	F	2.8	1.9	0.9	18.4	China desert	F	0.8	-1.6	-1.2	25.0
	M	4.0	-0.3	0.0	-18.7		M	-2.5	-0.9	-0.1	17.0
	S.D.-M	0.8	0.6	0.4	10.5		S.D.-F	1.0	0.5	0.3	6.0
Indian desert	F	4.5	0.7	0.5	8.2	Indian desert	F	-5.1	1.2	0.9	98.0
	M	3.1	0.5	0.6	4.6		M	-8.4	0.4	0.6	87.0
	S.D.-M	1.2	0.5	0.6	7.0		S.D.-F	0.5	0.2	0.2	0.7
Australian desert	F	4.9	0.2	0.1	1.1	Australian desert	F	-3.1	0.0	0.0	1.0
	M	5.3	0.0	0.1	-1.7		M	-3.8	-0.5	-0.1	-3.0
	S.D.-M	1.0	0.5	0.3	9.6		S.D.-F	0.7	0.1	0.1	0.5
Northern Sahara	F	5.1	0.2	0.2	0.1	Northern Sahara	F	-2.4	-0.3	-0.3	-1.0
	M	4.2	0.6	0.5	0.3		M	-3.1	0.3	0.2	1.0
	S.D.-M	0.7	0.3	0.3	0.2		S.D.-F	0.5	0.2	0.1	0.7
Southern Sahara	F	4.6	0.2	0.3	-1.1	Southern Sahara	F	-2.0	-0.7	-0.6	2.0
	M	3.5	0.8	0.7	1.6		M	-3.8	0.1	0.1	1.0
	S.D.-M	0.7	0.5	0.4	0.1		S.D.-F	0.2	0.3	0.2	0.7
African Sahel	F	4.6	0.3	0.4	-19.0	African Sahel	F	-3.0	-0.8	-0.4	4.0
	M	3.2	1.5	0.9	12.2		M	-3.3	0.1	0.0	14.0
	S.D.-M	0.6	0.5	0.4	7.0		S.D.-F	0.1	0.1	0.1	2.0
African rainforest	F	4.3	1.4	0.4	30.5	African rainforest	F	-3.3	0.7	0.0	41.0
	M	2.9	1.5	1.1	45.8		M	-3.9	1.0	0.5	68.0
	S.D.-M	0.3	0.5	0.3	11.1		S.D.-F	0.8	0.1	0.1	6.5
Amazon rainforest	F	4.9	-0.2	0.2	-44.1	Amazon rainforest	F	-3.0	-0.9	-0.2	-21.0
	M	4.1	0.1	0.2	-2.7		M	-4.1	1.0	1.1	85.0
	S.D.-M	0.6	0.4	0.4	11.1		S.D.-F	2.2	0.2	0.0	9.0

vided by the large-scale forcing of the ice sheets leads to somewhat greater similarity in results, at least in locations near the ice sheets. Considerable differences exist in regions further removed from the location of strong forcing. For example, for the southwestern United States, a region which experienced high lake levels during the ice age (Smith and Street-Perrott 1983), the fine grid shows an increase in summer precipitation while the medium grid shows a decrease. Summer precipitation depends strongly on the convective scheme, which is resolution dependent, as well as the ground hydrology parameterization, crudely handled in the control run.

There are variations with resolution in the ice age low-latitude effects, and it is of interest to readdress the question raised in Rind and Peteet (1985) of whether the low-latitude model results are in agreement with the terrestrial evidence of cooling. In that study, comparison was made of the model produced and observationally deduced cooling at four separate locations, Hawaii, East Africa, New Guinea and Colombia. While the paleoclimate terrestrial evidence suggested freezing line and vegetation zone reductions of 1 km, the medium-grid results provided reductions only one-half as large (and even less for Hawaii). The apparent discrepancy implied that the warm tropical and subtropical ocean temperatures indicated by the CLIMAP reconstruction were not consistent with the terrestrial implications. Is this result still true with the finer-grid ice age run? As shown above (Table 2), the finer-grid ice age run has greater reduction in atmospheric temperatures overall.

Comparisons have been made of the temperature profiles above each of the points in question. Over East Africa, Colombia, and New Guinea the results indicate that there are relatively small changes in the ice line descent as a function of resolution, on the order of ± 50 m. However, over Hawaii, the finer-grid ice line descends approximately 340 m, whereas in the medium-grid ice age run there is no descent at all. Reducing the CLIMAP prescribed sea surface temperatures by an additional 2°C brought the medium-grid model results into general conformity with the land evidence in all locations but Hawaii (Rind and Peteet 1985); the finer grid results imply that with that resolution, the effect might be sufficient for Hawaii as well. However, given the questions surrounding the performance of the moist convection scheme on the finer resolution, it is not at all apparent that the finer-resolution results are more accurate in this regard.

Finally, the question of ice mass balance, in both the ice age and doubled- CO_2 runs, can be examined for resolution dependency. The ice sheets 18 000 years ago in the medium-grid model were not in mass balance; as indicated in Rind (1987a), the imbalance for the continental ice sheets between 43° and 67°N , if translated directly into ice disappearance, would have

implied complete ice sheet removal in 1000–4000 years. When the same calculation is repeated with the finer grid (again, a somewhat colder run overall), the disappearance times increase to 1500–6000 years. This latter range is in somewhat better agreement with observations (up to 9000 years), although a direct comparison is unwarranted given the lack of a suitable ice dynamics model.

In Rind (1987b), the finer-grid doubled CO_2 climate mass balance for ice in Greenland and Antarctica was calculated from the resultant of runoff plus evaporation minus precipitation, compared to the control run values. Ice decreases of 1.4 mm d^{-1} over Greenland, and 0.1 to 0.5 mm d^{-1} for Antarctica resulted from the climate warming. With the medium grid, the value for Greenland turns out to be exactly the same, while the values for Antarctica fall within the range given above. In this case, the different resolution models are producing similar results.

5. Concluding remarks

Two major developments presently occurring in the climate modeling field are the utilization by various agencies and concerns of the future climate projections from current models, and the attempts of modeling groups to develop and use finer-resolution models. In this study, we have explored how climate change depictions might be altered with the use of different resolution models. The results show that major processes, such as the nonlinear energy transfer in the momentum equation and the convective sensitivity, differ substantially with two different resolutions of the GISS model, and that these differences, along with inherent difference in spatial scales, lead to resolution-dependent changes in atmospheric dynamics and regional climate. The users of model output should therefore be aware that important aspects of climate change depictions will likely vary as model resolution is altered. Disagreements are more probably in regions removed from the locations of strong climate change forcing, such as the ice sheets, and for parameters that are poorly reproduced—with significant resolution differences—for the current climate, such as summer precipitation.

The results also indicate that the higher-resolution model does not guarantee improvement in all processes. As it is reasonable to attach the most confidence to changes predicted by the most realistic model, this conclusion indicates that results from higher-resolution models should not be granted greater weight without a thorough investigation of the models' comparative climatologies. In particular, the zonal kinetic energy budget must be scrutinized, given the tendency of higher-resolution models to overestimate zonal winds. The current practice of incorporating additional drag mechanisms to counterbalance this effect should be weighed against the magnitude of the forcing terms;

for example, does the numerical solution of the momentum equation overestimate nonlinear energy transfers even when the additional drag mechanisms are in place? Climate changes are apparently very sensitive to model structure, so an apparently realistic model, produced with the use of improper parameterizations, will likely generate spurious results.

This study has focused on model resolution comparisons when the climate sensitivity, i.e., the sea surface temperature changes, are similar. For the doubled- CO_2 climate, the model sensitivities do in fact appear similar, but the medium-grid ice age sea surface temperatures would likely have cooled by $1^\circ\text{--}2^\circ\text{C}$ compared with the finer-grid results. This additional model dependency will alter climate change results even further, as will any substantial change in model physics or numerical scheme. The study described herein represents a prelude for what will likely become a major activity in climate change modeling.

Acknowledgments. Reto Reudy and Tristan Bukowski kindly helped in providing model diagnostic output. Leonard Druyan and Tony DelGenio offered useful comments in review. Climate modeling is supported by the NASA Climate Office and the Research and Development Office of the United States Environmental Protection Agency.

REFERENCES

- Arpe, K., and E. Klinker, 1986: Systematic errors of the ECMWF operational forecasting model in midlatitudes. *Quart. J. Roy. Meteor. Soc.*, **112**, 181–202.
- Baer, F., and F. N. Alyea, 1971: Effects of spectral truncation on general circulation and long-range prediction. *J. Atmos. Sci.*, **28**, 457–480.
- CLIMAP Project Members (A. McIntyre, project leader), 1981: Seasonal reconstruction of the earth's surface at the last glacial maximum. *Geol. Soc. Amer.*, Map and Chart Series, No. 36.
- Druyan, L., and D. Rind, 1988: Verification of regional climate of GISS GCM—Part 1: Winter. NASA Tech. Memo. 100695, 39 pp.
- Hansen, J., G. Russell, D. Rind, P. Stone, A. Lacis, S. Lebedeff, R. Reudy and L. Travis, 1983: Efficient three-dimensional global models for climate studies: Models I and II. *Mon. Wea. Rev.*, **111**, 609–662.
- , A. Lacis, D. Rind, G. Russell, P. Stone, I. Fung, R. Ruedy and J. Lerner, 1984: Climate sensitivity: Analysis of feedback mechanisms. *Climate Processes and Climate Sensitivity*, J. E. Hansen and T. Takahashi, Eds., Amer. Geophys. Union, 130–163.
- Hayashi, Y., and D. G. Golder, 1987: Effects of wave-wave and wave-mean flow interactions on the growth and maintenance of transient planetary waves in the presence of a mean thermal restoring force. *J. Atmos. Sci.*, **44**, 3392–3401.
- Hoke, J. E., 1987: Improving the horizontal resolution of the nested grid model. *National Weather Service Tech. Proc. Bull. No. 368*, 9 pp. [Available from the U.S. Dept. of Commerce.]
- Kutzbach, J. E., and B. L. Otto-Blieneser, 1982: The sensitivity of the African–Asian monsoonal climate to orbital parameter changes for 9000 years B.P. in a low-resolution general circulation model. *J. Atmos. Sci.*, **39**, 1177–1188.
- , and H. E. Wright, Jr., 1985: Simulation of the climate of 18,000 yr BP: Results for the North American/North Atlantic/European Sector. *Quart. Sci. Rev.*, **4**, 147–187.
- , and P. J. Guetter, 1986: The influence of changing orbital parameters and surface boundary conditions on climate simulations for the past 18,000 years. *J. Atmos. Sci.*, **43**, 1726–1759.
- Manabe, S., J. Smagorinsky, J. L. Holloway, Jr. and H. M. Stone, 1970: Simulated climatology of a general circulation model with a hydrologic cycle. Part III: Effects of increased horizontal computational resolution. *Mon. Wea. Rev.*, **98**, 175–212.
- , D. G. Hahn and J. L. Holloway, Jr., 1979: Climate simulations with GFDL spectral models of the atmosphere: Effect of spectral truncation. *Rep. of the JOC Study Conf. Climate Models: Performance, Intercomparison and Sensitivity Studies, Vol. 1*, W. L. Gates, Ed., GARP Publications Series No. 22, WMO, 41–94.
- McFarlane, N. A., 1987: The effect of orographically excited gravity wave drag on the general circulation of the lower stratosphere and troposphere. *J. Atmos. Sci.*, **44**, 1775–1800.
- Miller, J. R., G. L. Russell and L.-C. Tsang, 1983: Annual oceanic heat transports computed from an atmospheric model. *Dyn. Atmos. Oceans*, **7**, 95–109.
- Mitchell, J. F. B., C. A. Wilson and W. M. Cunningham, 1987: On CO_2 climate sensitivity and model dependence of results. *Quart. J. Roy. Meteor. Soc.*, **113**, 293–322.
- Miyakoda, K., R. F. Strickler, C. J. Nappo, P. L. Baker and G. D. Hembree, 1971: The effect of horizontal grid resolution in an atmospheric circulation model. *J. Atmos. Sci.*, **28**, 481–499.
- Oort, A. H., 1983: Global atmospheric circulation statistics, 1958–1973. NOAA Prof. Pap. 14, U.S. Dept. of Commerce, 180 pp. and 47 microfiches.
- , and E. Rasmusson, 1971: Atmospheric circulation statistics, NOAA Prof. Pap. 5, U.S. Dept. of Commerce, 323 pp.
- Palmer, T. N., and D. A. Mansfield, 1986: Wintertime circulation anomalies during past El Niño events, using a high resolution general circulation model. I: Influence of model climatology. *Quart. J. Roy. Meteor. Soc.*, **112**, 613–638.
- , G. J. Shutts and R. Swinbank, 1986: Alleviation of a systematic westerly bias in general circulation and numerical weather prediction models through an orographic gravity wave drag parameterization. *Quart. J. Roy. Meteor. Soc.*, **112**, 1001–1039.
- Rind, D., 1986: The dynamics of warm and cold climates. *J. Atmos. Sci.*, **43**, 3–24.
- , 1987a: Components of the ice age circulation. *J. Geophys. Res.*, **92**, 4241–4281.
- , 1987b: The doubled CO_2 climate: Impact of the sea surface temperature gradient. *J. Atmos. Sci.*, **44**, 3235–3268.
- , 1988: The doubled CO_2 climate and the sensitivity of the modeled hydrologic cycle. *J. Geophys. Res.*, **93**, 5385–5412.
- , and W. Rossow, 1984: The effects of physical processes on the Hadley circulation. *J. Atmos. Sci.*, **41**, 479–507.
- , and D. Peteet, 1985: Terrestrial conditions at the last glacial maximum and CLIMAP sea-surface temperature estimates: Are they consistent? *Quart. Res.*, **24**, 1–22.
- , R. Suozzo, N. K. Balachandran, A. Lacis and G. Russell, 1988: The GISS global climate/middle atmosphere model. Part I: Model structure and climatology. *J. Atmos. Sci.*, **45**, 329–370.
- Saltzman, B., 1970: Large-scale atmospheric energetics in the wave-number domain. *Rev. Geophys. Space Phys.*, **8**, 289–302.
- Schlesinger, M. E., and J. F. B. Mitchell, 1987: Climate model simulations of the equilibrium climatic response to increased carbon dioxide. *Rev. Geophys. Space Phys.*, **25**, 760–798.
- Smith, G. I., and Street-Perrott, F. A., 1983: Pluvial lakes of the western United States. *Late-Quaternary Environments of the United States. Vol. 1. The Late Pleistocene*, S. C. Porter, Ed., University of Minnesota Press, 190–214.
- Tenenbaum, J., 1987: Jet stream velocity errors in general circulation models. *Mon. Wea. Rev.*, **115**, 2744–2758.
- Wallace, J., and P. Hobbs, 1977: *Atmospheric Science*. Academic Press, 467 pp.
- Welck, R. E., A. Kasahara, W. M. Washington and G. de Santo, 1971: Effect of horizontal resolution in a fine-difference model of the general circulation. *Mon. Wea. Rev.*, **99**, 673–683.